

Falsifying Field-based Dark Energy Models

Genly Leon, Yoelsy Leyva, Emmanuel N. Saridakis,
Osmel Martin and Rolando Cardenas

November 21, 2018

Department of Mathematics,
Universidad Central de Las Villas, Santa Clara CP 54830, Cuba
Department of Physics,
Universidad Central de Las Villas, Santa Clara CP 54830, Cuba and
Department of Physics,
University of Athens, GR-15771 Athens, Greece
Email: genly@uclv.edu.cu, yoelsy@uclv.edu.cu, msaridak@phys.uoa.gr, osmel@uclv.edu.cu
and rcardenas@uclv.edu.cu

Abstract

We survey the application of specific tools to distinguish amongst the wide variety of dark energy models that are nowadays under investigation. The first class of tools is more mathematical in character: the application of the theory of dynamical systems to select the better behaved models, with appropriate attractors in the past and future. The second class of tools is rather physical: the use of astrophysical observations to crack the degeneracy of classes of dark energy models. In this last case the observations related with structure formation are emphasized both in the linear and non-linear regimes. We exemplify several studies based on our research, such as quintom and quinstant dark energy ones. Quintom dark energy paradigm is a hybrid construction of quintessence and phantom fields, which does not suffer from fine-tuning problems associated to phantom field and additionally it preserves the scaling behavior of quintessence. Quintom dark energy is motivated on theoretical grounds as an explanation for the crossing of the phantom divide, i.e. the smooth crossing of the dark energy state equation parameter below the value -1. On the other hand, quinstant dark energy is considered to be formed by quintessence and a negative cosmological constant, the inclusion of this later component allows for a viable mechanism to halt acceleration. We comment that the quinstant dark energy scenario gives good predictions for structure formation in the linear regime, but fails to do that in the non-linear one, for redshifts larger than one. We comment that there might still be some degree of arbitrariness in the selection of the best dark energy models.

Contents

1	Introduction	3
2	Observational Evidence for Quintom Dark Energy Paradigm	5
2.1	Basic observables	5
2.2	Perturbation theory and current observational constraints	8
2.2.1	Analysis of perturbations in quintom cosmology	8
2.2.2	Signatures of perturbations in quintom scenario	12
2.2.3	Breaking the degeneracy between quintom and cosmological constant scenarios	18
3	Exponential quintom: Phase space analysis	19
3.1	Flat FRW subcase	20
3.1.1	Analysis at infinity.	22
3.2	Models with negative curvature	24
3.2.1	Normalization, state space and dynamical system.	24
3.2.2	Form invariance under coordinate transformations.	25
3.2.3	Monotonic functions.	25
3.2.4	Local analysis of critical points.	26
3.2.5	Bifurcations.	28
3.2.6	Typical behavior.	28
3.3	Models with positive curvature	29
3.3.1	Normalization, state space and dynamical system.	29
3.3.2	Invariance under coordinate transformations.	30
3.3.3	Monotonic functions.	30
3.3.4	Local analysis of critical points.	31
3.3.5	Bifurcations.	33
3.3.6	Typical behaviour.	33
4	Observational Evidence for Quinstant Dark Energy Paradigm	35
4.1	The model	35
4.2	Matching with the data	35
4.2.1	The method and the data	36
4.2.2	Results	36
5	Exponential Quinstant: Phase space analysis	38
5.1	Flat FRW case	39
5.1.1	Normalization, state space, and dynamical system.	39
5.1.2	Form invariance under coordinate transformations.	40
5.1.3	Monotonic functions.	40
5.1.4	Local analysis of critical points.	40
5.1.5	Bifurcations.	45
5.1.6	Typical behavior	45
5.2	Quinstant cosmology with negative curvature	45
5.2.1	Normalization, state space, and dynamical system.	45

5.2.2	Form invariance under coordinate transformations.	46
5.2.3	Monotonic functions.	47
5.2.4	Local analysis of critical points.	47
5.2.5	Bifurcations.	49
5.2.6	Typical behavior.	49
5.3	Quinstant cosmology with positive curvature	53
5.3.1	Normalization, state space, and dynamical system.	53
5.3.2	Form invariance under coordinate transformations.	54
5.3.3	Monotonic functions	55
5.3.4	Local analysis of critical points.	55
5.3.5	Bifurcations.	57
5.3.6	Typical behavior.	57
6	Observational Test and Dynamical Systems: The Interplay	57

1 Introduction

The current accelerated expansion of our universe has been one of the most active fields in modern cosmology. Many cosmological models have been proposed to interpret this mysterious phenomenon, see e.g. [1, 2] for recent reviews. The simplest candidate is a positive cosmological constant Λ [3, 4]. It is well-known that its interpretation as the vacuum energy is problematic because of its exceedingly smallness [5]. Notwithstanding its observational merits, the Λ CDM scenario is seriously plagued by the well known coincidence and fine tuning problems [6] which are the main motivations to look for alternative models.

Dark energy (DE) models with two scalar fields (quintessence and phantom) have settled out explicitly and named quintom models [7, 8, 9, 10, 11, 12, 13, 14, 15, 16, 22, 23, 24, 25, 26, 27, 28, 29, 30]. The quintom paradigm is a hybrid construction of a quintessence component, usually modelled by a real scalar field that is minimally coupled to gravity, and a phantom field: a real scalar field –minimally coupled to gravity– with negative kinetic energy. Let us define the equation of state parameter of any cosmological fluid as $w \equiv \text{pressure/density}$. The simplest model of dark energy (vacuum energy or cosmological constant) is assumed to have $w = -1$. A key feature of quintom-like behavior is the crossing of the so called phantom divide, in which the equation of state parameter crosses through the value $w = -1$.¹ Quintom behavior (i.e., the $w = -1$ crossing) has been investigated in the context of h-essence cosmologies [14, 15]; in the context of holographic dark energy [17, 18, 19, 20, 21]; inspired by string theory [22, 23, 24]; derived from spinor matter [25]; for arbitrary potentials [27, 28, 29, 30]; using isomorphic models consisting of three coupled oscillators, one of which carries negative kinetic energy (particularly for investigating the dynamical behavior of massless quintom)[31]. The crossing of the phantom divide is also possible in the context of scalar tensor theories [32, 33, 34, 35, 36] as well as in modified theories of gravity [37].

¹In section 2 we refer briefly to observational evidence in favor the quintom DE model.

The cosmological evolution of quintom model with exponential potential has been examined, from the dynamical systems viewpoint, in [12] and [13, 16]. The difference between [12] and [13, 16] is that in the second case the potential considers the interaction between the conventional scalar field and the phantom field. In [13] it had been proven that in the absence of interactions, the solution dominated by the phantom field should be the attractor of the system and the interaction does not affect its attractor behavior. In [16] the case in which the interaction term dominates against the mixed terms of the potential, was studied. It was proven there, that the hypothesis in [13] is correct only in the cases in which the existence of the phantom phase excludes the existence of scaling attractors (in which the energy density of the quintom field and the energy density of DM are proportional). Some of this results were extended in [27], for arbitrary potentials. There it was settled down under what conditions on the potential it is possible to obtain scaling regimes. It was proved there, that for arbitrary potentials having asymptotic exponential behavior, scaling regimes are associated to the limit where the scalar fields diverge. Also it has been proven that the existence of phantom attractors in this framework is not generic and consequently the corresponding cosmological solutions lack the big rip singularity.

In the first part of the chapter we investigate basic cosmological observables of quintom paradigm. We perform the cosmological perturbations analysis of quintom model for independent quadratic potentials. We investigate the evolution of quintom cosmology with exponential potentials in a background of a comoving perfect uid. First, we review the at FRW subcase (with dust background). Then, we consider both negative and positive curvature FRW models. We construct two dynamical systems, one adapted to negative curvature and the other adapted to positive curvature. We characterize the critical points of the resulting systems. By devising well-defined monotonic functions we get global results for ever expanding and contracting models. We find the existence of orbits starting from and recollapsing to a singularity (given by a massless scalar field cosmology) for positive curvature models. There is also a closed FRW solution with no scalar field starting from a big-bang and recollapsing to a “big-crunch”. We have determined conditions for the existence of different types of global attractors. Furthermore, our monotonic functions rule out periodic orbits, recurrent orbits or homoclinic orbits. We comment about the interplay between dynamical analysis and observational checking as tools for discriminate among different quintom proposals.

A large variety of dark energy models suffers from the eternal acceleration problem, due to the exponential de-Sitter expansion. One of the consequences of the eternal acceleration is that a cosmic horizon appears (see e.g. [39] for a further discussion). This problem is not strictly related to Λ , should we replace Λ with a quintessence scalar field, the universe should still be eternally accelerated finally reaching a de Sitter phase and hence again a finite cosmic horizon. In the second part of the chapter we explore from both observational testing and dynamical systems perspective a theoretical model to address the horizon problem. We consider an effective dark energy fluid as a source of the

accelerated expansion. We follow a model presented by some of us [38, 39] whose dark energy component is the sum of a negative cosmological constant and a quintessence scalar field evolving under the action of an exponential potential². As a result, although the model is presently accelerating, eternal acceleration disappears and the universe ends in a Big Crunch like singularity in a finite time. Motivated by these theoretical virtues, we further explore this model from the observational point of view in order to see whether a negative Λ is indeed compatible with the astrophysical data at hand. We conclude that a negative Λ is indeed allowed and could represent a viable mechanism to halt eternal acceleration. We also explore the predictions of this class of model concerning the structure formation in the Universe. We conclude that this model give good predictions for structure formation in the linear regime, but fail to do so in the non-linear.

2 Observational Evidence for Quintom Dark Energy Paradigm

In this section we are going to refer briefly on the observational evidence that favor the quintom DE model.

2.1 Basic observables

In this subsection we examine the basic observational quantity, which is the dark energy (DE) Equation-of-State (EoS) parameter. In 2004, supernovae Ia data were accumulated, opening the road to constraint imposition on the time variation of DE EoS. In [44] uncorrelated and nearly model independent band power estimates (basing on the principal component analysis [45]) of the EoS of DE and its density as a function of redshift were presented, by fitting to the SNIa data. Quite unexpectedly, they found marginal (2σ) evidence for $w(z) < -1$ at $z < 0.2$, which is consistent with other results in the literature [46, 47, 48, 49, 50, 51].

The aforementioned result implied that the EoS of DE could indeed vary with time. Therefore, one could use a suitable parametrization of w_{DE} as a function of the redshift z , in order to satisfactory describe such a behavior. There are two well-studied parametrizations. The first (ansatz A) is:

$$w_{\text{DE}} = w_0 + w'z , \quad (1)$$

where w_0 the DE EoS at present and w' an additional parameter. However, this parametrization is only valid at low redshift, since it suffers from severe divergences at high ones, for example at the last scattering surface $z \sim 1100$. Therefore, a new, divergent-free ansatz (ansatz B) was proposed [52, 53]:

$$w_{\text{DE}} = w_0 + w_1(1 - a) = w_0 + w_1 \frac{z}{1+z} , \quad (2)$$

²another point of view of the composite dark energy models can be found in [40, 41, 42, 43] where the cosmon model is introduced

where a is the scale factor and $w_1 = -dw/da$. This parametrization exhibits a very good behavior at high redshifts.

In [54] the authors used the “gold” sample of 157 SNIa, the low limit of cosmic ages and the HST prior, as well as the uniform weak prior on $\Omega_m h^2$, to constrain the free parameters of above two DE parameterizations. As can be

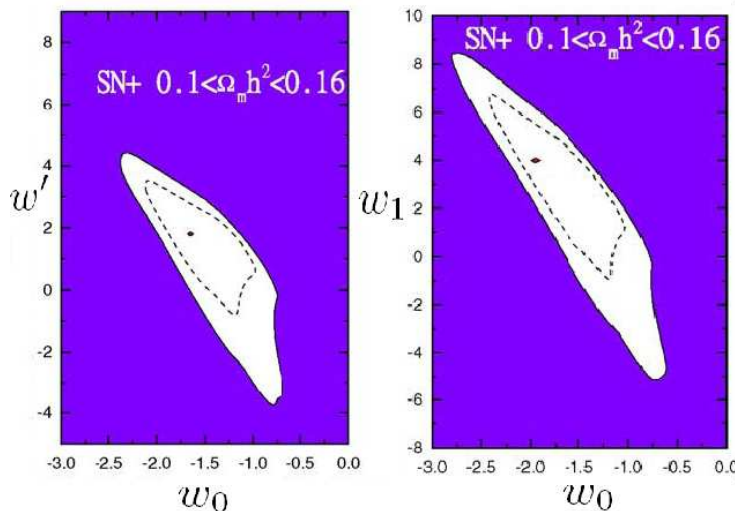


Figure 1: (Color online) *Two-dimensional contour-plots of the DE equation-of-state parameters, in two different parameterizations and using SNIa data. The left graph corresponds to ansatz A (expression (1)) and the right graph are to ansatz B (expression (2)). From Ref. [54].*

seen in Fig.1 they found that the data seem to favor an evolving DE with the EoS being below -1 around the present epoch, while it was in the range $w > -1$ in the near cosmological past. This result holds for both parameterizations (1),(2), and in particular the best fit value of the EoS at present is $w_0 < -1$, while its “running” coefficient is larger than 0.

Apart from the SNIa data, CMB and LSS data can be also used to study the variation of EoS of DE. In [55], the authors used the first year WMAP, SDSS and 2dFGRS data to constrain different DE models. They indeed found that evidently the data favor a strongly time-dependent w_{DE} , and this result is consistent with similar project of the literature [56, 57, 58, 59, 60, 61, 62, 63, 64, 65]. Using the latest 5-year WMAP data, combined with SNIa and BAO data, the constraints on the DE parameters of ansatz B are: $w_0 = -1.06 \pm 0.14$ and $w_1 = 0.36 \pm 0.62$ [68, 66, 67], and the corresponding contour plot is presented in Fig.2.

In conclusion, as can be observed, the current observational data mildly favor w_{DE} crossing the phantom divide during the evolution of universe.

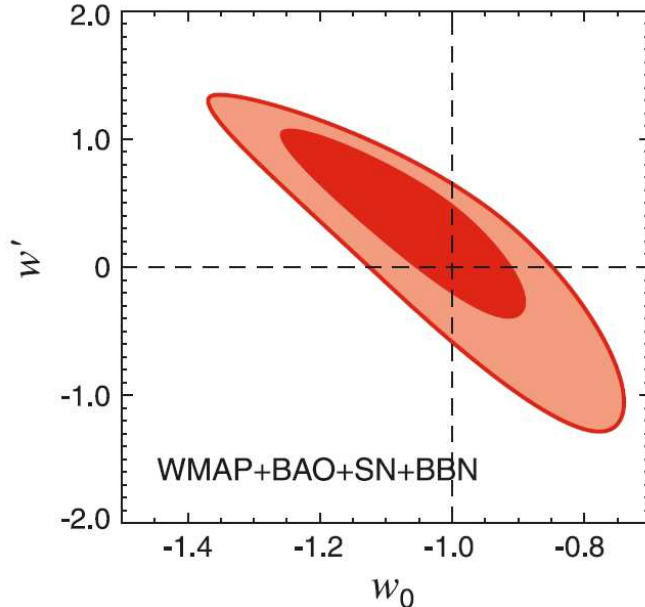


Figure 2: (Color online) *Two-dimensional contour-plot of the DE equation-of-state parameters, in parameterization ansatz B (expression (2)), and using WMAP, BAO, SNIa data. From Ref. [68].*

Let us make some comments here. First of all, we mention that the above results can also fit the basic Λ CDM paradigm, where dark energy is attributed to the simple cosmological constant. Thus, many authors believe that according to data resolution we can still trust the Λ CDM paradigm, and thus there is no need to introduced additional and more complex mechanisms. The second comment is the following: even if we accept that the results seem to favor a DE EoS below -1 at present, this does not necessarily means that a two field explanation (one canonical and one phantom, i.e the basic quintom model) is automatically justified. One can still result to $w_0 < -1$ through many different frameworks including modified gravity, braneworld constructions, stringy or strong-inspired models, spinor models etc [69]. Thus, in order to distinguish between these alternatives, one has to find more complicated signatures of the two-filed quintom model, apart from the simple observable of DE EoS. One step towards this direction is to investigate the perturbation spectrum of two-field quintom model, and then examine its relation to observations.

2.2 Perturbation theory and current observational constraints

In this subsection we study the perturbations of two-field quintom DE paradigm and the effects of these perturbations on the current observations. Additionally, since it is important to check the consistency of this model at the classical level, it requires us to analyze the behavior of perturbations when the EoS crosses the cosmological constant boundary [70].

2.2.1 Analysis of perturbations in quintom cosmology

In the following discussion on the quintom perturbations we will restrict ourselves to the two-field quintom model, with a Lagrangian:

$$\mathcal{L} = \mathcal{L}_Q + \mathcal{L}_P, \quad (3)$$

where

$$\mathcal{L}_Q = \frac{1}{2} \partial_\mu \phi_1 \partial^\mu \phi_1 - V_1(\phi_1) \quad (4)$$

describes the canonical (quintessence) component, and

$$\mathcal{L}_P = -\frac{1}{2} \partial_\mu \phi_2 \partial^\mu \phi_2 - V_2(\phi_2) \quad (5)$$

the phantom one. The equations of motion for the two scalar fields $\phi_i (i = 1, 2)$ read

$$\ddot{\phi}_i + 2\mathcal{H}\dot{\phi}_i \pm a^2 \frac{\partial V_i}{\partial \phi_i} = 0, \quad (6)$$

where the positive sign is for the quintessence and the minus sign for the phantom field. Although in general the two scalar fields could be coupled with each other, here for simplicity we neglect these interactions.

Now, for a complete study on the perturbations, apart from the fluctuations of the fields, one has to consider also the metric perturbations. In the conformal Newtonian gauge the perturbed metric writes

$$ds^2 = a^2(\tau)[(1 + 2\Psi)d\tau^2 - (1 - 2\Phi)dx^i dx_i]. \quad (7)$$

Using the notation of [71], the perturbation equations satisfied by each of the quintom components are:

$$\dot{\delta}_i = -(1 + w_i)(\theta_i - 3\dot{\Phi}) - 3\mathcal{H} \left(\frac{\delta P_i}{\delta \rho_i} - w_i \right) \delta_i, \quad (8)$$

$$\dot{\theta}_i = -\mathcal{H}(1 - 3w_i)\theta_i - \frac{\dot{w}_i}{1 + w_i}\theta_i + k^2 \left(\frac{\delta P_i / \delta \rho_i}{1 + w_i} \delta_i - \sigma_i + \Psi \right), \quad (9)$$

where

$$\theta_i = (k^2 / \dot{\phi}_i) \delta \phi_i, \quad \sigma_i = 0, \quad (10)$$

$$w_i = \frac{P_i}{\rho_i}, \quad (11)$$

and

$$\delta P_i = \delta \rho_i - 2V_i' \delta \phi_i = \delta \rho_i + \frac{\rho_i \theta_i}{k^2} [3\mathcal{H}(1 - w_i^2) + \dot{w}_i]. \quad (12)$$

Thus, combining Eqs. (8), (9) and (12), we obtain

$$\dot{\theta}_i = 2\mathcal{H}\theta_i + \frac{k^2}{1 + w_i} \delta_i + k^2 \Psi, \quad (13)$$

$$\dot{\delta}_i = -(1 + w_i)(\theta_i - 3\dot{\Phi}) - 3\mathcal{H}(1 - w_i)\delta_i - 3\mathcal{H} \left[\frac{\dot{w}_i + 3\mathcal{H}(1 - w_i^2)}{k^2} \right] \theta_i. \quad (14)$$

Since the simple two-field quintom model is essentially a combination of a quintessence and a phantom field, one obtains the perturbation equations by combining the aforementioned equations. The corresponding variables for the quintom system are

$$w_{quintom} = \frac{\sum_i P_i}{\sum_i \rho_i}, \quad (15)$$

$$\delta_{quintom} = \frac{\sum_i \rho_i \delta_i}{\sum_i \rho_i}, \quad (16)$$

and

$$\theta_{quintom} = \frac{\sum_i (\rho_i + p_i) \theta_i}{\sum_i (\rho_i + P_i)}. \quad (17)$$

Note that for the quintessence component, $-1 \leq w_1 \leq 1$, while for the phantom component, $w_2 \leq -1$.

The two-field quintom model is characterized by the potentials V_i . Lets us not consider the simplified case of quadratic potentials $V_i(\phi_i) = \frac{1}{2} m_i^2 \phi_i^2$. In general the perturbations of ϕ_i arise from two origins, namely from the adiabatic and the isocurvature modes. Using instead of δ_i the gauge invariant variable $\zeta_i = -\Phi - \mathcal{H} \frac{\delta \rho_i}{\rho_i}$, and in addition the relation $\Phi = \Psi$ in a universe without anisotropic stress, the equations (14) and (13) can be rewritten as,

$$\dot{\zeta}_i = -\frac{\theta_i}{3} - C_i \left(\zeta_i + \Phi + \frac{\mathcal{H}}{k^2} \theta_i \right) \quad (18)$$

$$\dot{\theta}_i = 2\mathcal{H}\theta_i + k^2(3\zeta_i + 4\Phi), \quad (19)$$

where

$$C_i = \frac{\dot{w}_i}{1 + w_i} + 3\mathcal{H}(1 - w_i) = \partial_0[\ln(a^6 |\rho_i + p_i|)]. \quad (20)$$

In these expressions ζ_i is the curvature perturbation on the uniform-density hypersurfaces for the i -component of the universe [72]. Usually, the isocurvature perturbations of ϕ_i are characterized by the differences between the curvature

perturbation of the uniform- ϕ_i -density hypersurfaces and that of the uniform-radiation-density hypersurfaces,

$$S_{ir} \equiv 3(\zeta_i - \zeta_r), \quad (21)$$

where the subscript r stands for radiation. Here we assume there are no matter isocurvature perturbations, and thus $\zeta_m = \zeta_r$. Eliminating ζ_i in equations (18) and (19), we obtain a second order equation for θ_i , namely

$$\ddot{\theta}_i + (C_i - 2\mathcal{H})\dot{\theta}_i + (C_i\mathcal{H} - 2\dot{\mathcal{H}} + k^2)\theta_i = k^2(4\dot{\Phi} + C_i\Phi). \quad (22)$$

The general solutions of this inhomogeneous differential equation, is the sum of the general solution of its homogeneous part with a special integration. In the following, we will show that the special integration corresponds to the adiabatic perturbation.

As it assumed, before the era of DE domination, the universe was dominated by either radiation or dark matter. The perturbation equations for these background fluids read:

$$\begin{aligned} \dot{\zeta}_f &= -\theta_f/3, \\ \dot{\theta}_f &= -\mathcal{H}(1 - 3w_f)\theta_f + k^2[3w_f\zeta_f + (1 + 3w_f)\Phi]. \end{aligned} \quad (23)$$

From the Poisson equation

$$-\frac{k^2}{\mathcal{H}^2}\Phi = \frac{9}{2} \sum_{\alpha} \Omega_{\alpha}(1 + w_{\alpha}) \left(\zeta_{\alpha} + \Phi + \frac{\mathcal{H}}{k^2}\theta_{\alpha} \right) \simeq \frac{9}{2}(1 + w_f) \left(\zeta_f + \Phi + \frac{\mathcal{H}}{k^2}\theta_f \right), \quad (24)$$

on large scales we approximately acquire:

$$\Phi \simeq -\zeta_f - \frac{\mathcal{H}}{k^2}\theta_f. \quad (25)$$

Therefore, combining the equations above with $\mathcal{H} = 2/[(1 + 3w_f)\tau]$, we get (note that numerically $\theta_f \sim \mathcal{O}(k^2)\zeta_f$)

$$\begin{aligned} \zeta_f &= -\frac{5 + 3w_f}{3(1 + w_f)}\Phi = \text{const.}, \\ \theta_f &= \frac{k^2(1 + 3w_f)}{3(1 + w_f)}\Phi\tau. \end{aligned} \quad (26)$$

Therefore, from (22) we observe that there is a special solution which on large scales it is given approximately by

$$\theta_i^{ad} = \theta_f, \quad (27)$$

while (19) leads to

$$\zeta_i^{ad} = \zeta_f. \quad (28)$$

This indicates that the special integration of (22) corresponds to the adiabatic perturbation. Hence, concerning the isocurvature perturbations of ϕ_i , we can consider only the solution to the homogeneous part of (22),

$$\ddot{\theta}_i + (C_i - 2\mathcal{H})\dot{\theta}_i + (C_i\mathcal{H} - 2\dot{\mathcal{H}} + k^2)\theta_i = 0. \quad (29)$$

These solutions are represented by θ_i^{iso} and ζ_i^{iso} . The relation between them is

$$\zeta_i^{iso} = \frac{\dot{\theta}_i^{iso} - 2\mathcal{H}\theta_i^{iso}}{3k^2}. \quad (30)$$

Since the general solution of ζ_i is

$$\zeta_i = \zeta_i^{ad} + \zeta_i^{iso} = \zeta_r + \zeta_i^{iso}, \quad (31)$$

the isocurvature perturbations are simply $S_{ir} = 3\zeta_i^{iso}$.

In order to solve (29), we need to know the forms of C_i and \mathcal{H} as functions of time τ . For this purpose, we solve the background equations (6). During the radiation dominated period, $a = A\tau$, $\mathcal{H} = 1/\tau$ and we thus we have

$$\phi_1 = \tau^{-1/2} \left[A_1 J_{1/4} \left(\frac{A}{2} m_1 \tau^2 \right) + A_2 J_{-1/4} \left(\frac{A}{2} m_1 \tau^2 \right) \right], \quad (32)$$

and

$$\phi_2 = \tau^{-1/2} \left[\tilde{A}_1 I_{1/4} \left(\frac{A}{2} m_2 \tau^2 \right) + \tilde{A}_2 I_{-1/4} \left(\frac{A}{2} m_2 \tau^2 \right) \right], \quad (33)$$

respectively, where A , A_i and \tilde{A}_i are constants, $J_\nu(x)$ is the ν th order Bessel function and $I_\nu(x)$ is the ν th order modified Bessel function. Since the masses are usually small in comparison with the expansion rate of the early universe $m_i \ll \mathcal{H}/a$, we can approximate the (modified) Bessel functions as $J_\nu(x) \sim x^\nu(c_1 + c_2x^2)$ and $I_\nu(x) \sim x^\nu(\tilde{c}_1 + \tilde{c}_2x^2)$. We mention that $J_{-1/4}$ and $I_{-1/4}$ are divergent when $x \rightarrow 0$. Given these arguments we can see that it requires large initial values of ϕ_i and $\dot{\phi}_i$ if A_2 and \tilde{A}_2 are not vanished. Imposing small initial values, which is the natural choice if the DE fields are assumed to survive after inflation, only A_1 and \tilde{A}_1 modes exist, so $\dot{\phi}_i$ will be proportional to τ^3 in the leading order. Thus, the parameters C_i in (20) will be $C_i = 10/\tau$ (we have used $|\rho_i + \tilde{p}_i| = \dot{\phi}_i^2/a^2$). So, we acquire the solution of (29),

$$\theta_i^{iso} = \tau^{-4} [D_{i1} \cos(k\tau) + D_{i2} \sin(k\tau)]. \quad (34)$$

Therefore, θ_i^{iso} presents an oscillatory behavior, with an amplitude damping with the expansion of the universe. This fact leads the isocurvature perturbations ζ_i^{iso} to decrease rapidly. If we choose large initial values for ϕ_i and $\dot{\phi}_i$, A_2 and \tilde{A}_2 modes are present, $\dot{\phi}_i$ will be proportional to τ^{-2} in the leading order and $C_i = 0$. Now the solution of (29) is:

$$\theta_i^{iso} = \tau [D_{i1} \cos(k\tau) + D_{i2} \sin(k\tau)]. \quad (35)$$

That is, θ_i^{iso} will oscillate with an increasing amplitude, so ζ_i^{iso} remains constant on large scales.

Similarly, during matter dominated era, $a = B\tau^2$, $\mathcal{H} = 2/\tau$, and thus the solutions for the fields ϕ_i respectively read

$$\phi_1 = \tau^{-3} \left[B_1 \sin \left(\frac{B}{3} m_1 \tau^3 \right) + B_2 \cos \left(\frac{B}{3} m_1 \tau^3 \right) \right] \quad (36)$$

and

$$\phi_2 = \tau^{-3} \left[\tilde{B}_1 \sinh \left(\frac{B}{3} m_2 \tau^3 \right) + \tilde{B}_2 \cosh \left(\frac{B}{3} m_2 \tau^3 \right) \right]. \quad (37)$$

Therefore, we do get the same conclusions with the analysis for the radiation dominated era. Firstly, choosing small initial values at the beginning of matter domination, we deduce that the isocurvature perturbations in ϕ_i will decrease with time. On the contrary, for large initial values, the isocurvature perturbations remain constant on large scales. This behavior was expected, since in the case of large initial velocity the energy density of the scalar field is dominated by the kinetic term and it behaves like a fluid with $w = 1$, and thus its isocurvature perturbation remains constant on large scales. However, on the other hand, the energy density of the scalar field will be dominated by the potential energy due to the slow rolling, that is it will behave like a cosmological constant and thus there are only tiny isocurvature perturbations in it.

In summary, we have seen that the isocurvature perturbations in quintessence-like or phantom-like field under quadratical potentials decrease or remain constant at large scales, depending on the initial velocities. In other words, the isocurvature perturbations are stable on large scales, with their amplitude being proportional to the value of Hubble parameter evaluated during the period of inflation H_{inf} (if indeed their quantum nature originates from inflation). In the case of a large H_{inf} , the isocurvature dark energy perturbations can be non-negligible and thus they will contribute to the observed CMB anisotropy [73, 74]. However, in the cases analyzed in this subsection, these isocurvature perturbations are negligible. Firstly, as mentioned above, large initial velocities are not possible if we desire the quintom fields to survive after inflation. Furthermore, even if the initial velocities are large at the beginning of the radiation domination, they will be reduced to a small value due to the small masses and the damping effect of Hubble expansion.

In conclusion, we deduce that the contributions of DE isocurvature perturbations are not very large [75] and thus for simplicity we assume that H_{inf} is small enough in order to make the isocurvature contributions negligible. Therefore, it is safe to focus only in the effects of the adiabatic perturbations of the quintom model.

2.2.2 Signatures of perturbations in quintom scenario

Let us now investigate the observational signatures of perturbations in quintom scenario. For this sake we use the perturbation equations(16) and (17), and we

are based on the code of CAMB [76]. For simplicity we impose a flat geometry as a background, although this is not necessary. Moreover, we assume the fiducial background parameters to be $\Omega_b = 0.042$, $\Omega_{DM} = 0.231$, $\Omega_{DE} = 0.727$, where b stands for baryons, DM for dark matter and DE for dark energy, while today's Hubble constant is fixed at $H_0 = 69.255 \text{ km/s Mpc}^{-2}$. We will calculate the effects of perturbed quintom on CMB and LSS.

In the two-field quintom model there are two parameters, namely the quintessence and phantom masses. When the quintessence mass is larger than the Hubble parameter, the field starts to oscillate and consequently one obtains an oscillating quintom. In the numerical analysis we will fix the phantom mass to be $m_P \sim 2.0 \times 10^{-60} M_{pl}$, and we vary the quintessence mass with the typical values being $m_Q = 10^{-60} M_{pl}$ and $4 \times 10^{-60} M_{pl}$ respectively.

Oscillatory Quintom

In Fig. 3 we depict the equation-of-state parameters as a function of the scale factor, for the aforementioned two parameter-sets, and additionally their corresponding effects on observations. We clearly observe the quintom oscillating behavior as the mass of quintessence component increases. After reaching the $w = -1$ pivot for several times, w crosses -1 consequently with the phantom-component domination in dark energy. As a result, the quintom fields modifies the metric perturbations: $\delta g_{00} = 2a^2\dot{\Psi}$, $\delta g_{ii} = 2a^2\Phi\delta_{ij}$ and consequently they contribute to the late-time Integrated Sachs-Wolfe (ISW) effect. The ISW effect is an integrant of $\dot{\Phi} + \dot{\Psi}$ over conformal time and wavenumber k . The above two specific quintom models yield quite different evolving $\Phi + \Psi$ as shown in the right panel of Fig. 3, where the scale is $k \sim 10^{-3} \text{ Mpc}^{-1}$. As we can see, the late time ISW effects differ significantly when DE perturbations are taken into account (solid lines) or not (dashed lines).

ISW effects constitute an important part on large angular scales of CMB and on the matter power spectrum of LSS. For a constant EoS of phantom it has been shown that the low multipoles of CMB will get significantly enhanced when DE perturbations are neglected [77]. On the other hand for a matter-like scalar field, where the EoS is around zero, perturbations will also play an important role on the large scales of CMB [78]. Our results on CMB and LSS reflect the two combined effects of phantom and oscillating quintessence. We mention that while in the early studies of quintessence effects on CMB, one could consider a constant w_{eff} instead:

$$w_{eff} \equiv \frac{\int da \Omega(a) w(a)}{\int da \Omega(a)} \quad , \quad (38)$$

this is not enough for the study of effects on SNIa, nor for CMB, when the EoS of DE has a very large variation with redshift, such as the model of oscillating quintom considered above.

To analyze the oscillating quintom-model under the current observations, we perform a preliminary fitting to the first year WMAP TT and the TE temperature-polarization cross-power spectrum as well as the recently released

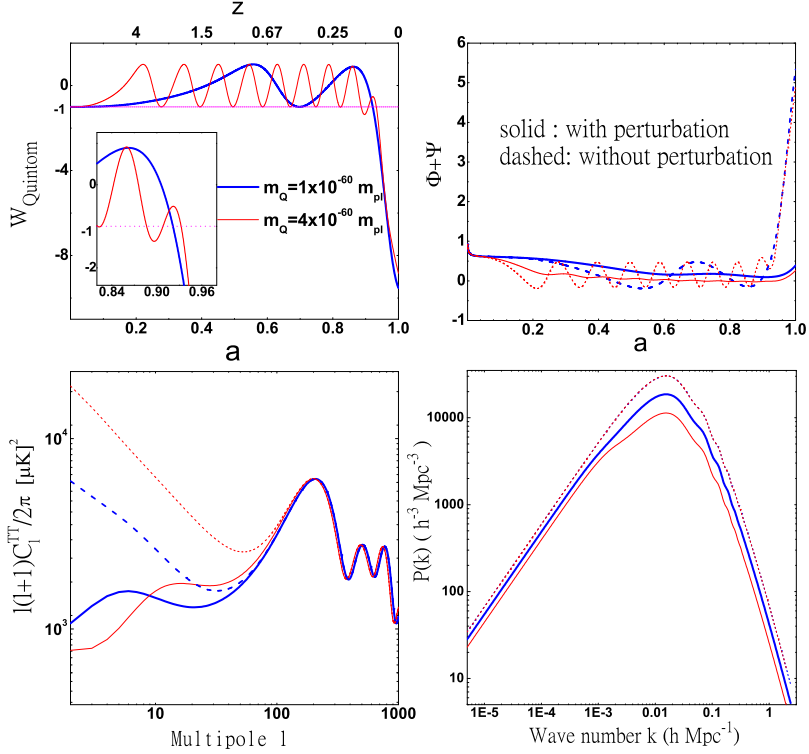


Figure 3: (Color online) *Effects of the two-field oscillating quintom on the observables. The phantom mass is fixed at $2.0 \times 10^{-60} M_{\text{pl}}$ and the quintessence mass at $10^{-60} M_{\text{pl}}$ (thicker line) and $4.0 \times 10^{-60} M_{\text{pl}}$ (thinner line) respectively. The upper right graph depicts the evolution of the metric perturbations $\Phi + \Psi$ of the two models, with (solid lines) and without (dashed lines) DE perturbations. The scale is $k \sim 10^{-3} \text{ Mpc}^{-1}$. The lower left graph shows the CMB effects and the lower right one delineates the effects on the matter power-spectrum, with (solid lines) and without (dashed lines) DE perturbations. From Ref. [70].*

157 “Gold” SNIa data [79]. Following [80, 81] in all the fittings below we fix $\tau = 0.17$, $\Omega_m h^2 = 0.135$ and $\Omega_b h^2 = 0.022$, setting the spectral index as $n_S = 0.95$, and using the amplitude of the primordial spectrum as a continuous parameter. In the fittings of oscillating quintom we’ve fixed the phantom-mass to be $m_P \sim 6.2 \times 10^{-61} M_{pl}$. Fig. 4 delineates 3σ WMAP and SNIa constraints on the two-field quintom model, and in addition it shows the corresponding best fit values. The parameters m_Q and m_P stand for the masses of quintessence and phantom respectively. In the left graph of Fig.4 we present the separate WMAP and SNIa constraints. The green(shaded) area is WMAP constraints on models where DE perturbations have been included, while the blue area (contour with solid lines) is the corresponding area without DE perturbations. The perturbations of DE have no effects on the geometric constraint of SNIa. The right graph shows the combined WMAP and SNIa constraints on the two-field quintom model with perturbations (green/shaded region) and without perturbations (red region/contour with solid lines). We conclude that the confidence regions indeed present a large difference, if the DE perturbations have been taken into account or not.

Non-oscillatory Quintom

As we have mentioned, the basic observables could also be described by the simple cosmological constant. Thus, in order to distinguish the quintom model from the cosmological constant, we now consider a quintom scenario where w crosses -1 smoothly without oscillations. It is interesting to study the effects of this type of quintom model, with its effective EoS defined in (38) exactly equal to -1 , on CMB and matter power spectrum. Indeed, we have realized such a quintom model in the lower right panel of Fig. 5, which can be easily given in the two-field model with a lighter quintessence mass. In this example we have set $m_Q \sim 2.6 \times 10^{-61} M_{pl}$, $m_P \sim 6.2 \times 10^{-61} M_{pl}$. Additionally, we assume that there is no initial kinetic energy. The initial value of the quintessence component is set to $\phi_{1i} = 0.226 M_{pl}$, while for the phantom part we impose $\phi_{2i} = 6.64 \times 10^{-3} M_{pl}$. We find that the EOS of quintom crosses -1 at $z \sim 0.15$, which is consistent with the latest SNIa results.

The model of quintom, which is mainly favored by current SNIa only, needs to be confronted with other observations in the framework of concordance cosmology. Since SNIa offer the only direct detection of DE, this model is the most promising to be distinguished from the cosmological constant and other dynamical DE models which do not get across -1 , by future SNIa projects on the low redshift (for illustrations see e.g. [44]). This is also the case for the quintom model in the full parameter space: it can be most directly tested in low redshift Type Ia supernova surveys.

In the upper left panel of Fig. 5 we delineate the different ISW effects among the cosmological constant (red/light solid), the quintom model which gives $w_{eff} = -1$ with (blue/dark solid) and without (blue dashed) perturbations. Similarly to the previous oscillating case, the difference is very large when switching off quintom perturbations and much smaller when including the

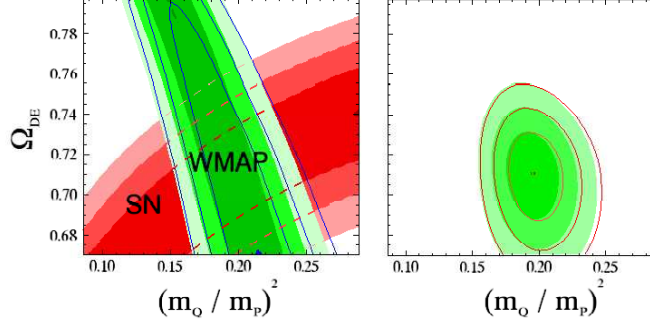


Figure 4: (Color online) 3σ WMAP and SNIa constraints on two-field quintom model, shown together with the best fit values. m_Q and m_P denote the quintessence and phantom mass respectively. We have fixed $m_P \sim 6.2 \times 10^{-61} M_{pl}$ and we have varied the value of m_Q . Left graph: separate WMAP and SNIa constraints. The green (shaded) area marks the WMAP constraints on models where DE perturbations have been included, while the blue area (contour with solid lines) corresponds to the case where DE perturbations have not been taken into account. Right graph: combined WMAP and SNIa constraints on the two-field quintom model with perturbations (green/shaded region) and without perturbations (red region/contour with solid lines). From Ref. [70].

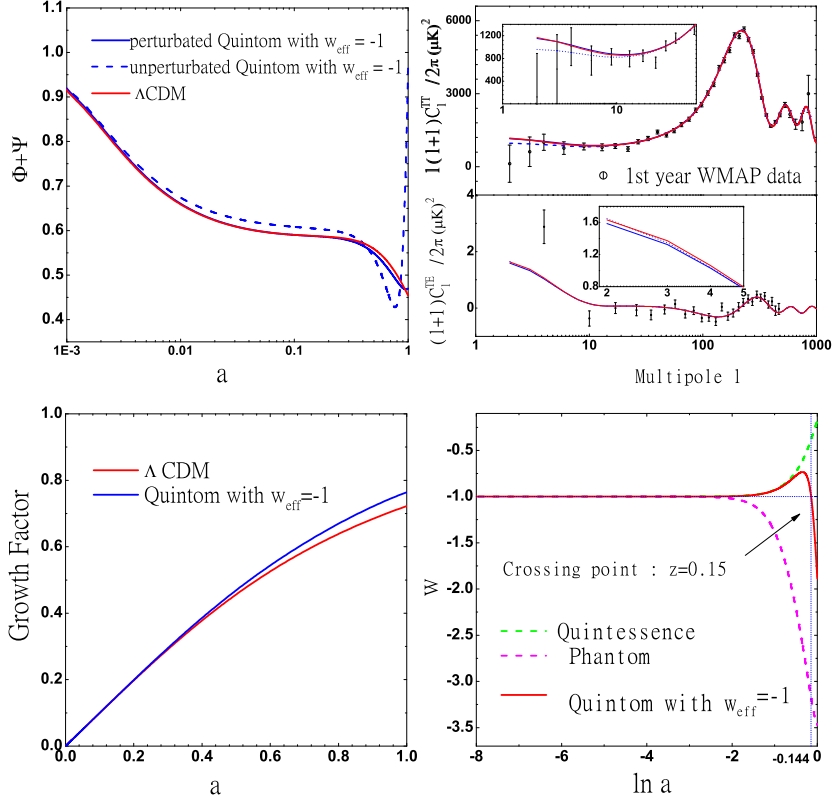


Figure 5: (Color online) Comparison of the effects of the two-field quintom model with $w_{\text{eff}} = -1$ and of the simple cosmological constant, in CMB (WMAP), the metric perturbations $\Phi + \Psi$ (the scale is $k \sim 10^{-3} \text{ Mpc}^{-1}$) and the linear growth factor. The binned error bars in the upper right graph are WMAP TT and TE data [82, 83]. From Ref. [70].

perturbations. In the upper right panel we find that the quintom model cannot be distinguished from a cosmological constant in light of WMAP. The two models give almost exactly the same results in CMB TT and TE power spectra when including the perturbations. We deduce that the difference in CMB is hardly distinguishable even by cosmic variance.

2.2.3 Breaking the degeneracy between quintom and cosmological constant scenarios

So far we have seen that CMB observations cannot distinguish between a quintom model with $w_{eff} = -1$ and a cosmological constant. Thus, in order to acquire distinctive signatures, we have to rely in other observations. To achieve that we need to consider the physical observables which can be affected by the evolving w sensitively. In comparison with the cosmological constant, such a quintom model exhibits a different evolution of the universe's expansion history, and in particular it gives rise to a different epoch of matter-radiation equality. The Hubble expansion parameter becomes:

$$H \equiv \frac{\dot{a}}{a^2} = H_0[\Omega_m a^{-3} + \Omega_r a^{-4} + X]^{1/2} \quad (39)$$

where X , the energy density ratio of DE between the early times and today, is quite different between the *quintom*-CDM and Λ CDM. In the Λ CDM scenario X is simply a constant, while in general for DE models with varying energy density or EoS we obtain

$$X = \Omega_{DE} a^{-3} e^{-3 \int w(a) d \ln a}. \quad (40)$$

Therefore, the two models will give different Hubble expansion rates. This is also the case between the quintom model with $w_{eff} = -1$ in the left panel of Fig. 5 and a cosmological constant.

Finally, we mention that different H leads directly to different behaviors of the growth factor. In particular, according to the linear perturbation theory all Fourier modes of the matter density perturbations grow at the same rate, that is the matter density perturbations are independent of k :

$$\ddot{\delta}_k + \mathcal{H} \dot{\delta}_k - 4\pi G a^2 \rho_M \delta_k = 0. \quad (41)$$

The growth factor $D_1(a)$ characterizes the growth of the matter density perturbations, namely $D_1(a) = \delta_k(a)/\delta_k(a=1)$, and it is normalized to unity today. In the matter-dominated epoch we have $D_1(a) = a$. Analytically $D_1(a)$ is often approximated by the Meszaros equation [84]:

$$D_1(a) = \frac{5\Omega_m H(a)}{2H_0} \int_0^a \frac{da'}{(a'H(a')/H_0)^3}. \quad (42)$$

Therefore, we can easily observe the difference between the quintom and cosmological constant scenarios, due to the different Hubble expansion rates. In

particular, one needs to solve (41) numerically. In the lower left graph of Fig. 5 we show the difference of $D_1(a)$ between the quintom model with $w_{eff} = -1$ and the cosmological constant one. The difference in the linear growth function is considerably large in the late time evolution and possibly distinguishable in future LSS surveys and in weak gravitational lensing (WGL) observations. WGL has emerged with a direct mapping of cosmic structures and it has been recently shown that the method of cosmic magnification tomography can be extremely efficient [85, 86, 87], which leaves a promising future for breaking the degeneracy between quintom and a cosmological constant.

3 Exponential quintom: Phase space analysis

In the following discussion on the quintom phase space analysis we restrict ourselves to the two-field quintom model, with a Lagrangian:

$$\mathcal{L} = \frac{1}{2}\partial_\mu\phi\partial^\mu\phi - \frac{1}{2}\partial_\mu\varphi\partial^\mu\varphi - V(\phi, \varphi), \quad (43)$$

and we include, also, ordinary matter (a comoving perfect fluid) in the gravitational action. As in [16] we consider here the effective two-field potential

$$V = V_0 e^{-\sqrt{6}(m\phi+n\varphi)}, \quad (44)$$

where the scalar field ϕ represents quintessence and φ represents a phantom field. For simplicity, we assume $m > 0$ and $n > 0$.

Quintom (non-conventional) cosmologies with exponential potentials has been investigated, from the dynamical systems approach, for instance, in references [12, 13, 16] (see section 3.1 for a brief review).

We shall consider the Friedmann-Lemaitre-Robertson-Walker (FLRW) line element:

$$ds^2 = -dt^2 + a^2(t) \left(\frac{dx^2}{1-kx^2} + x^2 (d\vartheta^2 + \sin^2\vartheta d\varphi^2) \right), \quad (45)$$

where $k = 1, 0, -1$, identifies the three types of FRW universes: closed, flat, and open, respectively.

The field equations derived from (45), are

$$H^2 - \frac{1}{6} \left(\dot{\phi}^2 - \dot{\varphi}^2 \right) - \frac{1}{3} V_{\text{eff}} - \frac{1}{3} \rho_M = -\frac{k}{a^2}, \quad (46)$$

$$\dot{H} = -H^2 - \frac{1}{3} \left(\dot{\phi}^2 - \dot{\varphi}^2 \right) + \frac{1}{3} V_{\text{eff}} - \frac{1}{6} \rho_M, \quad (47)$$

$$\dot{\rho}_M = -3H\rho_M, \quad (48)$$

$$\ddot{\phi} + 3H\dot{\phi} - \sqrt{6}mV = 0, \quad (49)$$

$$\ddot{\varphi} + 3H\dot{\varphi} + \sqrt{6}nV = 0, \quad (50)$$

where $H = \frac{\dot{a}(t)}{a(t)}$ denotes de Hubble expansion scalar.

The dot denotes derivative with respect the time t . We consider a pressureless perfect fluid (dust) as the background matter.

3.1 Flat FRW subcase

To investigate the flat models we introduced the same normalized variables as in [16]: (x_ϕ, x_φ, y) , defined by

$$x_\phi = \frac{\dot{\phi}}{\sqrt{6H}}, \quad x_\varphi = \frac{\dot{\varphi}}{\sqrt{6H}}, \quad y = \frac{\sqrt{V}}{\sqrt{3H}}. \quad (51)$$

They are related through the Friedman equation 46 by $x_\phi^2 - x_\varphi^2 + y^2 = 1 - \frac{\rho_M}{3H^2} \leq 1$.

The dynamics in the space is given by the ordinary differential equations [16]:

$$x'_\phi = \frac{1}{3} (3my^2 + (q-2)x_\phi) \quad (52)$$

$$x'_\varphi = -\frac{1}{3} (3ny^2 - (q-2)x_\varphi) \quad (53)$$

$$y' = \frac{1}{3} (1 + q - 3(mx_\phi + nx_\varphi))y \quad (54)$$

defined in the phase space given by

$$\Psi = \{\mathbf{x} = (x_\phi, x_\varphi, y) : 0 \leq x_\phi^2 - x_\varphi^2 + y^2 \leq 1\}. \quad (55)$$

Here the prime denotes differentiation with respect to a new time variable $\tau = \log a^3$, where a is the scale factor of the space-time. The deceleration factor $q \equiv -\ddot{a}/\dot{a}^2$ can then be written

$$q = \frac{1}{2} (3(x_\phi^2 - x_\varphi^2 - y^2) + 1). \quad (56)$$

The system (52-54) admits the critical points O, C_\pm, T, P reported in [16]). In the table 1 the location, existence and deceleration factor of the critical points for $m > 0, n > 0$ and $y > 0$. We use the notation $\delta = m^2 - n^2$.

By analyzing the sign of the real part of the normally-hyperbolic curves C_\pm we get the following results (we are assuming $m > 0$ and $n > 0$):

- If $m < n$, C_+ contains an infinite arc parameterized by x_φ^* such that $x_\varphi^* < \frac{-n-m\sqrt{1-\delta}}{\delta}$ that is a local source. C_- contains an infinite arc parameterized by x_φ^* such that $x_\varphi^* < \frac{-n+m\sqrt{1-\delta}}{\delta}$ that is a local source.
- If $m = n$, C_+ contains an infinite arc parameterized by x_φ^* such that $x_\varphi^* < \frac{1-m^2}{2n}$ that is a local source. All of C_- is a local source.
- If $m > n$ there are two possibilities
 - If $\delta < 1$, all of C_- is a local source. A finite arc of C_+ parameterized by x_φ^* such that $\frac{-n-m\sqrt{1-\delta}}{\delta} < x_\varphi^* < \frac{-n+m\sqrt{1-\delta}}{\delta}$ is a local source.

Table 1: Location, existence and deceleration factor of the critical points for $m > 0$, $n > 0$ and $y > 0$. We use the notation $\delta = m^2 - n^2$ (from reference [16]).

Name	x_ϕ	x_φ	y	Existence	q
O	0	0	0	All m and n	$\frac{1}{2}$
C_\pm	$\pm\sqrt{1+x_\varphi^{*2}}$	x_φ^*	0	All m and n	2
P	m	$-n$	$\sqrt{1-\delta}$	$\delta < 1$	$-1+3\delta$
T	$\frac{m}{2\delta}$	$-\frac{n}{2\delta}$	$\frac{1}{2\sqrt{\delta}}$	$\delta \geq 1/2$	$\frac{1}{2}$

– If $\delta \geq 1$, no part of C_+ is a local source and all of C_- is a local source.

Perhaps, the most appealing result in [16] is that, by introducing properly defined monotonic functions and by making some numerical integrations, it was possible to identify heteroclinic sequences

- Case i) For $m < \sqrt{n^2 + 1/2}$, the point P is a stable node, whereas the point T does not exist. The heteroclinic sequence in this case is $C_\pm \rightarrow O \rightarrow P$.
- Case ii) For $\sqrt{n^2 + 1/2} < m \leq \sqrt{n^2 + 4/7}$, the point T is a stable node and the point P is a saddle. For these conditions the heteroclinic sequence is $C_\pm \rightarrow O \rightarrow T \rightarrow P$.
- Case iii) For $\sqrt{n^2 + 4/7} < m < \sqrt{1 + n^2}$, the point T is a spiral node and the point P is a saddle. For these conditions the heteroclinic sequence is the same as in the former case.
- Case iv) For $m > \sqrt{1 + n^2}$ the point T is a spiral node whereas the point P does not exist. The heteroclinic sequence in this case is $C_- \rightarrow O \rightarrow T$.

From the possibilities listed above, there still the possibility of other attractors different from phantom ones in the exponential quintom scenario, particularly scaling attractors (T). This fact is a counterexample of one of the result in [13]. However, we are aware on the small probability that T represents the actual stage on the universe evolution due this solution is matter-dominated. Another compelling result in quintom cosmology is that the existence of monotonic functions in the state space can rule out periodic orbits, homoclinic orbits, and other complex behaviour in invariant sets. If so, the dynamics is dominated by critical points (and possibly, heteroclinic orbits joining it). Additionally, some global results can be obtained. A similar approach (i.e., that of devising monotonic functions) for multiple scalar field cosmologies with matter was used

Table 2: Location and existence conditions for the critical points at infinity.

Name	θ_1	θ_2	Existence
P_1^\pm	0	$\pm \frac{\pi}{2}$	always
P_2^\pm	π	$\pm \frac{\pi}{2}$	always
P_3^\pm	$\frac{\pi}{4}$	$\pm \cos^{-1}\left(-\frac{m}{n}\right)$	$-\pi < \pm \cos^{-1}\left(-\frac{m}{n}\right) \leq \pi, n \neq 0$
P_4^\pm	$\frac{3\pi}{4}$	$\pm \cos^{-1}\left(\frac{m}{n}\right)$	$-\pi < \pm \cos^{-1}\left(\frac{m}{n}\right) \leq \pi, n \neq 0$
P_5	θ_1^*	0	$0 \leq \theta_1^* \leq \pi$
P_6	θ_1^*	π	$0 \leq \theta_1^* \leq \pi$

in [88, 89, 90]. However, in that work they do not consider phantom-like scalar fields, as we do here.

3.1.1 Analysis at infinity.

The numerical experiments in [16] suggest that there is an open set of orbits that tends to infinity. Let us investigate the dynamics at infinity. In order to do that we will use the central Poincaré projection method. Thus, to obtain the critical points at infinity we introduce spherical coordinates (ρ is the inverse of $r = \sqrt{x_\phi^2 + x_\varphi^2 + y^2}$, then, $\rho \rightarrow 0$ as $r \rightarrow \infty$):

$$x_\phi = \frac{1}{\rho} \sin \theta_1 \cos \theta_2, \quad (57)$$

$$y = \frac{1}{\rho} \sin \theta_1 \sin \theta_2, \quad (58)$$

$$x_\varphi = \frac{1}{\rho} \cos \theta_1 \quad (59)$$

where $0 \leq \theta_1 \leq \pi$ and $-\pi < \theta_2 \leq \pi$, and $0 < \rho < \infty$.

Defining the time derivative $f' \equiv \rho \dot{f}$, the system (52-54), can be written as

$$\rho' = \frac{1}{2} (\cos^2 \theta_1 - \cos(2\theta_2) \sin^2 \theta_1) + 2n \cos \theta_1 \sin^2 \theta_1 \sin^2 \theta_2 \rho + O(\rho^2). \quad (60)$$

and

$$\begin{aligned} \theta_1' &= n \cos(2\theta_1) \sin \theta_1 \sin^2 \theta_2 - \cos \theta_1 \sin \theta_1 \sin^2 \theta_2 \rho + O(\rho^2), \\ \theta_2' &= (n \cos \theta_1 \cos \theta_2 + m \sin \theta_1) \sin \theta_2 - \cos \theta_2 \sin \theta_2 \rho + O(\rho^2). \end{aligned} \quad (61)$$

Table 3: Stability of the critical points at infinity. We use the notation $\delta = m^2 - n^2$ and $\lambda^\pm = n \cos \theta_1^* \pm m \sin \theta_1^*$.

Name	(λ_1, λ_2)	ρ'	Stability
P_1^\pm	$(-n, n)$	> 0	saddle
P_2^\pm	$(-n, n)$	> 0	saddle
P_3^\pm	$\left(\frac{\sqrt{2}\delta}{n}, \frac{\delta}{\sqrt{2}n}\right)$	$\begin{cases} > 0, & \delta < 0 \\ < 0, & \delta > 0 \end{cases}$	source if $n < 0, n < m < -n$ saddle otherwise
P_4^\pm	$\left(-\frac{\sqrt{2}\delta}{n}, -\frac{\delta}{\sqrt{2}n}\right)$	$\begin{cases} > 0, & \delta < 0 \\ < 0, & \delta > 0 \end{cases}$	source if $n > 0, -n < m < n$ saddle otherwise
P_5	$(0, \lambda^+)$	$\begin{cases} < 0, & \frac{\pi}{4} < \theta_1^* < \frac{3\pi}{4} \\ > 0, & \text{otherwise} \end{cases}$	nonhyperbolic
P_6	$(0, \lambda^-)$	$\begin{cases} < 0, & \frac{\pi}{4} < \theta_1^* < \frac{3\pi}{4} \\ > 0, & \text{otherwise} \end{cases}$	nonhyperbolic

Since equation (60) does not depend on the radial component at the limit $\rho \rightarrow 0$, we can obtain the critical points at infinity by solving equations (61) in the limit $\rho \rightarrow 0$. Thus, the critical points at infinity must satisfy the compatibility conditions

$$\begin{aligned} \cos(2\theta_1) \sin \theta_1 \sin^2 \theta_2 &= 0, \\ (n \cos \theta_1 \cos \theta_2 + m \sin \theta_1) \sin \theta_2 &= 0. \end{aligned} \quad (62)$$

First, we examine the stability of the pairs (θ_1^*, θ_2^*) satisfying the compatibility conditions (62) in the plane θ_1 - θ_2 , and then, we examine the global stability by substituting in (60) and analyzing the sign of $\rho'(\theta_2^*, \theta_2^*)$. In table 2 it is offered information about the location and existence conditions of these critical points. In table 3 we summarize the stability properties of these critical points.

Let us describe the cosmological solutions associated with the critical points at infinity.

The cosmological solutions associated to the critical points P_1^\pm and P_2^\pm have the evolution rates $\dot{\phi}^2/V = 0$, $\dot{\phi}/\dot{\varphi} = 0$ and $H/\dot{\varphi} \equiv \rho/\sqrt{6} \rightarrow 0$.³ These solutions are always saddle points at infinity. The critical points P_3^\pm and P_4^\pm are sources provided $n < 0, n < m < -n$ or $n > 0, -n < m < n$, respectively. They are saddle points otherwise. The associated cosmological solutions

³Do not confuse ρ with the matter energy density, the latter denoted by ρ_M .

to P_3^\pm have the evolution rates $\dot{\phi}^2/V = \frac{2m^2}{n^2-m^2}$, $\dot{\phi}/\dot{\varphi} = -m/n$, and $H/\dot{\phi} \equiv -n\rho/(\sqrt{3}m) \rightarrow 0$, and $H/\dot{\varphi} \equiv \rho/\sqrt{3} \rightarrow 0$, whereas the associated cosmological solutions to P_4^\pm have the evolution rates $\dot{\phi}^2/V = \frac{2m^2}{n^2-m^2}$, $\dot{\phi}/\dot{\varphi} = -m/n$, and $H/\dot{\phi} \equiv n\rho/(\sqrt{3}m) \rightarrow 0$, and $H/\dot{\varphi} \equiv -\rho/\sqrt{3} \rightarrow 0$. The curves of critical points P_5 and P_6 are nonhyperbolic. The associated cosmological solutions have expansion rates (valid for $\theta_1^* \neq \pi/4$) $V/\dot{\phi}^2 = 0$, $\dot{\phi}/\dot{\varphi} = \tan \theta_1^*$, $H/\dot{\phi} = \rho \sec \theta_1^*/\sqrt{6} \rightarrow 0$, and $V/\dot{\varphi}^2 = 0$, $\dot{\phi}/\dot{\varphi} = -\tan \theta_1^*$, $H/\dot{\varphi} = \rho \sec \theta_1^*/\sqrt{6} \rightarrow 0$, respectively.

3.2 Models with negative curvature

In this section we investigate negative curvature models.

3.2.1 Normalization, state space and dynamical system.

For the investigation of negative curvature models we shall use the normalized variables: $(x_\phi, x_\varphi, y, \Omega)$, defined by

$$x_\phi = \frac{\dot{\phi}}{\sqrt{6}H}, \quad x_\varphi = \frac{\dot{\varphi}}{\sqrt{6}H}, \quad y = \frac{\sqrt{V}}{\sqrt{3}H}, \quad \Omega = \frac{\rho_M}{3H^2}. \quad (63)$$

This choice allows to recast the Friedmann equation (46) as

$$1 - (x_\phi^2 - x_\varphi^2 + y^2 + \Omega) = \Omega_k \geq 0, \quad (64)$$

where

$$\Omega_k = -\frac{k}{a^2 H^2}, \quad k = -1, 0. \quad (65)$$

Thus,

$$0 \leq x_\phi^2 - x_\varphi^2 + y^2 + \Omega \leq 1. \quad (66)$$

Let us introduce the new time variable, τ , such that $\tau \rightarrow -\infty$ as $t \rightarrow 0$ and $\tau \rightarrow +\infty$ as $t \rightarrow +\infty$. Since the time direction must be preserved we can choose $d\tau = 3\epsilon H dt$ where $\epsilon = \pm 1 = \text{sign}(H)$.

The field equations (63) are

$$\begin{aligned} x_\phi' &= \epsilon \left(\frac{1}{3} (q-2) x_\phi + m y^2 \right), \\ x_\varphi' &= \epsilon \left(\frac{1}{3} (q-2) x_\varphi - n y^2 \right), \\ y' &= \epsilon \left(\frac{1}{3} (1+q) - m x_\phi - n x_\varphi \right) y, \\ \Omega' &= \frac{1}{3} \epsilon (2q-1) \Omega. \end{aligned} \quad (67)$$

Where $q = 2 \left(x_\phi^2 - x_\varphi^2 \right) - y^2 + \frac{1}{2} \Omega$, is the expression for the deceleration parameter. The DE EoS parameter, w , can be rewritten, in terms of the phase variables, as

$$w = \frac{x_\phi^2 - x_\varphi^2 - y^2}{x_\phi^2 - x_\varphi^2 + y^2}. \quad (68)$$

Table 4: Coordinates and existence conditions for the critical points of the system 67. We have used the notation $\delta = m^2 - n^2$. The subindexes in the labels have the following meaning: the left subindex (denoted by $\epsilon = \pm 1$) indicates when the model is expanding (+) or contracting (-); the right subindex denotes the sign of x_ϕ (i.e., the sign of ϕ) and it is displayed by the sign \pm .

Label	Coordinates: ($x_\phi, x_\varphi, y, \Omega$)	Existence
$\pm K_\pm$	$(\pm\sqrt{1+x_\varphi^*{}^2}, x_\varphi^*, 0, 0)$	All m and n
$\pm M$	$(0, 0, 0, 0)$	All m and n
$\pm F$	$(0, 0, 0, 1)$	All m and n
$\pm SF$	$(m, -n, \epsilon\sqrt{1-\delta}, 0)$	$\delta < 1$
$\pm CS$	$(\frac{m}{3\delta}, -\frac{n}{3\delta}, \frac{\epsilon\sqrt{2}}{3\sqrt{\delta}}, 0)$	$\delta > \frac{1}{3}$
$\pm MS$	$(\frac{m}{2\delta}, -\frac{n}{2\delta}, \frac{\epsilon\sqrt{1-\delta}}{2\sqrt{\delta}}, \sqrt{1-\frac{1}{2\delta}})$	$\delta > \frac{1}{2}$

Notice that the evolution equation (67 c) is form invariant under the coordinate transformation $y \rightarrow \epsilon y$. Then, the sign of ϵy is invariant by proposition 4.1 in [91], in such way that we can assume, without lost generality, for fixed ϵ , $\epsilon y \geq 0$. Hence, for each choice of sign of ϵ , the equations (67) define a flow in the phase space

$$\Psi^\pm = \{(x_\phi, x_\varphi, y, \Omega) : 0 \leq x_\phi^2 - x_\varphi^2 + y^2 + \Omega \leq 1, \\ x_\phi^2 - x_\varphi^2 + y^2 \geq 0, \Omega \geq 0, \epsilon y \geq 0\}. \quad (69)$$

3.2.2 Form invariance under coordinate transformations.

First recall that the positive “branch” ($\epsilon = +1$) describe the dynamics of models ever expanding and the negative “branch” ($\epsilon = -1$) describes the dynamics for contracting models. The system is form invariant under the change $\epsilon \rightarrow -\epsilon$, i.e., the system is symmetric under time-reversing. In this way it is enough to characterize the dynamics in Ψ^+ .

3.2.3 Monotonic functions.

Let be defined in the phase space Ψ^+ (or Ψ^- , depending of the choice of ϵ) the function

Table 5: DE EoS parameter (w), deceleration parameter (q), fractional energy densities, and eigenvalues of the perturbation matrix associated to the critical points of the system 67. We use the notation $\lambda^\pm = nx_\phi^* \pm m\sqrt{1+x_\phi^{*2}}$. $\pm K_\pm$, $\pm F$, $\pm SF$ $\pm MS$ corresponds to $k = 0$, the eigenvalues of these points in the invariant set of zero-curvature models are the same as displayed in the table but the first from the left.

Label	w	q	$\Omega_m, \Omega_{de}, \Omega_k$	Eigenvalues
$\pm K_\pm$	1	2	0, 1, 0	$\frac{4}{3}\epsilon, 0, \epsilon(1 - \lambda^\pm), \epsilon$
$\pm M$	-	0	0, 0, 1	$-\frac{2}{3}\epsilon, -\frac{2}{3}\epsilon, \frac{1}{3}\epsilon, -\frac{1}{3}\epsilon$
$\pm F$	-	$\frac{1}{2}$	1, 0, 0	$\frac{1}{2}\epsilon, -\frac{1}{2}\epsilon, -\frac{1}{2}\epsilon, \frac{1}{3}\epsilon$
$\pm SF$	$-1 + 2\delta$	$-1 + 3\delta$	0, 1, 0	$2(\delta - \frac{1}{3})\epsilon, (\delta - 1)\epsilon, (\delta - 1)\epsilon, (2\delta - 1)\epsilon$
$\pm CS$	$-\frac{1}{3}$	0	$0, \frac{1}{3\delta}, 1 - \frac{1}{3\delta}$	$-\frac{2}{3}\epsilon, -\frac{1}{3}\epsilon, -\frac{1}{3}\left(\epsilon \pm \sqrt{\frac{4}{3\delta} - 3}\right)$
$\pm MS$	0	$\frac{1}{2}$	$1 - \frac{1}{2\delta}, \frac{1}{2\delta}, 0$	$\frac{1}{3}\epsilon, -\frac{1}{2}\epsilon, -\frac{1}{4}\left(\epsilon \pm \sqrt{-7 + \frac{4}{\delta}}\right)$

$$M = \frac{(nx_\phi + mx_\phi)^2 \Omega^2}{(1 - x_\phi^2 + x_\phi^2 - y^2 - \Omega)^3}, \quad M' = -2\epsilon M. \quad (70)$$

This is a monotonic function for $\Omega > 0$ and $nx_\phi + mx_\phi \neq 0$. Then, the existences of such monotonic function rule out periodic orbits, recurrent orbits, or homoclinic orbits in the phase space and also, there is possible global results from the local stability analysis of critical points. Additionally, from the expression of M one can see immediatly that $\Omega \rightarrow 0$, or $nx_\phi + mx_\phi \rightarrow 0$ o $|nx_\phi + mx_\phi| \rightarrow +\infty$ (implying x_ϕ or x_ϕ or both diverge) or $\Omega_k \rightarrow 0$ asymptotically.

3.2.4 Local analysis of critical points.

By the discussion about the invariance of the system, it is sufficient characterize dynamically the critical points $+K_\pm$, $+M$, $+F$ $+SF$ $+CS$ y $+MS$, in the phase space Ψ^+ . In tables 4 and 5, it is offered information about the location, existence and eigenvalues of the critical points of the system (67) in the phase space (69) (for each choice of ϵ) and also, it is displayed the values of some cosmological parameters associated to the corresponding cosmological solutions.

Now we shall investigate the local stability of the critical points (and curves of critical points). We shall characterize de associated cosmological solutions.

The set of critical points $\pm K_{\pm}$ and the isolated critical points $\pm M$ are located in the invariant set of massless scalar field (MSF) cosmologies without matter. The isolated critical points $\pm F$ are located in the invariant set of MSF cosmologies with matter.

The arcs of hyperbolae $\pm K_{\pm}$ parameterized by the real value x_{φ}^* denote cosmological models dominated by the energy density of DE ($\Omega_{de} \rightarrow 1$), particularly by its kinetic energy. DE mimics a stiff fluid solution. Since this are a set of critical points, then necessarily, they have a zero eigenvalue. They are local sources (and in general they constitute the past attractor in the phase space Ψ^+) provided $nx_{\varphi}^* \pm m\sqrt{1 + x_{\varphi}^{*2}} < 1$.

The isolated critical points $\pm M$ denote the Milne's universe. They are non-hyperbolic. The critical points $\pm F$ represent flat FRW solutions (dominated by matter). They are hyperbolic. For this points the quintom field vanishes, then, the DE's cosmological parameters are not applicable to this points.

The stable manifold of $+M$ is 3-dimensional and it is tangent at the point to the 3-dimensional space $(x_{\phi}, x_{\varphi}, \Omega)$ whereas the unstable one is 1-dimensional and tangent to the axis y . This means the the critical point $+M$ is unstable to perturbations in y . The critical point $+F$ have a 2-dimensional stable manifold tangent at the point to the plane (x_{ϕ}, x_{φ}) and a 2-dimensional unstable manifold tangent at the critical point to the plane (y, Ω) .

The isolated critical points $\pm SF$ and $\pm CS$ denotes cosmological solutions dominated by quintom dark energy and curvature scaling solutions, respectively. These are located in the invariant set of MSF cosmologies without matter ($\Omega = 0$). The critical points $\pm MS$ (belonging to the invariant set of MSF cosmologies with matter ($\Omega > 0$)) represent flat matter scaling solutions.

The stable manifold of $+SF$ in Ψ^+ is 4-dimensional provided $\delta < 1/3$. In this case $+SF$ is the global attractor on Ψ^+ . $+SF$ is a saddle with a 3-dimensional stable manifold, if $\frac{1}{3} < \delta < \frac{1}{2}$ or 2-dimensional if $\frac{1}{2} < \delta < 1$.

The isolated critical points $\pm CS$ are non-hyperbolic if $\delta = \frac{1}{3}$. On the other hand, the critical points $\pm MS$ are non-hyperbolic if $\delta = \frac{1}{2}$.

$+CS$ is stable (with a 4-dimensional stable manifold) and then, it is a global attractor provided $\frac{1}{3} < \delta \leq \frac{4}{9}$ (in this case all the eigenvalues are real) or if $\delta > \frac{4}{9}$ (in which case there exists two complex conjugated eigenvalues in such way that the orbits initially at the subspace spanned by the corresponding eigenvectors spiraling toward the critical point).

Let us notice that $+MS$ is the global attractor of the system (it have a 4-dimensional stable manifold) only if $0 < \gamma < \frac{2}{3}$, $\delta > \frac{2}{7}$ (where γ denotes the barotropic index of the perfect fluid). Since we are assuming $\gamma = 1$ (i.e., dust background) then, the critical point $+MS$ is a saddle. It have a 3-dimensional stable manifold if $\frac{1}{2} < \delta \leq \frac{4}{7}$ (in which case all the eigenvalues are real) or if $\delta > \frac{4}{7}$ (in which case there are two complex conjugated eigenvalues and then the orbits initially at the subspace spanned by the corresponding eigenvalues spiral in towards the critical point).

3.2.5 Bifurcations.

Observe that the critical points $\pm MS$ and $\pm SF$ are the same as $\delta \rightarrow \frac{1}{2}^+$. $+SF$ ($-SF$) coincide with a point in the arc $+K_+$ ($-K_-$) as $\delta \rightarrow 1^-$. This values of δ where the critical points coincide correspond to bifurcations since the stability changes.

3.2.6 Typical behavior.

Once the attractors have been identified one can give a quantitative description of the physical behaviour of a typical open ($k = -1$) quintom cosmology. For example, for ever expanding cosmologies, near the initial singularity the model behave as de flat FRW with stiff fluid (DE mimics a stiff fluid) represented by a critical point in $+K_+$ or in $+K_-$, depending on the selection of the free parameters m, n and x_φ^* (see table 6). Whenever $+CS$ exists (i.e., provided $\delta > \frac{1}{3}$) it is the global attractor of the system. In absence of this type of points, i.e., if $\delta < \frac{1}{3}$, the late time dynamics is determined by the critical point $+SF$, i.e., the universe will be accelerated, almost flat ($\Omega_k \rightarrow 0$) and dominated by DE ($\Omega_{de} \rightarrow 1$). DE behaves like quintessence ($-1 < q < 0$, i.e., $-1 < w < -\frac{1}{3}$) or a phantom field ($q < -1$, i.e., $w < -1$) if $\delta > 0$ or $\delta < 0$, respectively. This means that, typically, the ever expanding open quintom model crosses the phantom divide (DE EoS parameter have values less than -1).⁴ The intermediate dynamics will be governed by the critical points $+CS$, $+MS$, $y +M$, which have the highest lower-dimensional stable manifold.

Table 6: Summary of attractors of the system 67. Observe that, whenever exists, the solution dominated by curvature $-CS$ ($+CS$) is the past (the future) attractor for $\epsilon = -1$, i. e., for contracting models ($\epsilon = 1$, i.e., for expanding models). We use the notation $\lambda^\pm = nx_\varphi^* \pm m\sqrt{1 + x_\varphi^{*2}}$.

Restrictions	Past attractor	Future attractor
$\epsilon = -1$	$-SF$ if $\delta < \frac{1}{3}$	
	$-CS$ if $\delta > \frac{1}{3}$	$-K_\pm$ if $\lambda^\pm > -1$
$\epsilon = 1$		$+SF$ if $\delta < \frac{1}{3}$
	$+K_\pm$ if $\lambda^\pm < 1$	$+CS$ if $\delta > \frac{1}{3}$

For contracting models, the typical behavior, is in some way, the reverse of

⁴For flat models, is well known the, whenever it exists, (i.e., provided $\delta > \frac{1}{2}$) the attractor is $+MS$ (denoted by T in [16]). When we include curvature, the stability of the matter scaling solution is transferred to the curvature scaling solution, as we prove here.

the above. If $\delta < \frac{1}{3}$ the early time dynamics is dominated by $_{-}CS$. Otherwise, if $\delta > \frac{1}{3}$, the past attractor is $_{-}SF$, i.e., the model is accelerating, close to flatness ($\Omega_k \rightarrow 0$) and dominated by DE. The intermediate dynamics is dominated at large extent by the critical points $_{-}CS$, $_{-}MS$, y $_{-}F$, which have the highest lower-dimensional stable manifold. A typical model behaves at late times as a flat FRW universe with stiff fluid (i.e., ME mimics a stiff fluid) represented by the invariant sets $_{-}K_+$ or $_{-}K_-$, depending on the choice of the values of the free parameters m, n y x_φ^* .

3.3 Models with positive curvature

In this section we investigate positive curvature models we shall make use of the variables similar but not equal to those defined in [88] section VI.A.

3.3.1 Normalization, state space and dynamical system.

Let us introduce the normalization factor

$$\hat{D} = 3\sqrt{H^2 + a^{-2}}. \quad (71)$$

Observe that

$$\hat{D} \rightarrow 0 \Leftrightarrow H \rightarrow 0, a \rightarrow +\infty$$

(i.e., at a singularity). This means that it is not possible that \hat{D} vanishes at a finite time.

Let us introduce the following normalized variables $(Q_0, \hat{x}_\phi, \hat{x}_\varphi, \hat{y}, \hat{\Omega})$, given by

$$Q_0 = \frac{3H}{\hat{D}}, \hat{x}_\phi = \sqrt{\frac{3}{2}} \frac{\dot{\phi}}{\hat{D}}, \hat{x}_\varphi = \sqrt{\frac{3}{2}} \frac{\dot{\varphi}}{\hat{D}}, \hat{y} = \frac{\sqrt{3}V}{\hat{D}}, \hat{\Omega} = \frac{3\rho_M}{\hat{D}^2}. \quad (72)$$

From the Friedmann equation we find

$$0 \leq \hat{x}_\phi^2 - \hat{x}_\varphi^2 + \hat{y}^2 = 1 - \hat{\Omega} \leq 1 \quad (73)$$

and by definition

$$-1 \leq Q_0 \leq 1. \quad (74)$$

By the restrictions (73, 74), the state variables are in the state space

$$\hat{\Psi} = \{(Q_0, \hat{x}_\phi, \hat{x}_\varphi, \hat{y}) : 0 \leq \hat{x}_\phi^2 - \hat{x}_\varphi^2 + \hat{y}^2 \leq 1, -1 \leq Q_0 \leq 1\}. \quad (75)$$

As before, this state space is not compact.

Let us introduce the time coordinate

$$' \equiv \frac{d}{d\hat{\tau}} = \frac{3}{\hat{D}} \frac{d}{dt}.$$

\hat{D} has the evolution equation

$$\hat{D}' = -3Q_0\hat{D} \left(\hat{x}_\phi^2 - \hat{x}_\varphi^2 + \frac{1}{2}\hat{\Omega} \right)$$

where

$$\hat{\Omega} = 1 - (\hat{x}_\phi^2 - \hat{x}_\varphi^2 + \hat{y}).$$

This equation decouples from the other evolution equations. Thus, a reduced set of evolution equations is obtained.

$$\begin{aligned} Q_0' &= (1 - Q_0^2) (1 - 3\Xi), \\ \hat{x}_\phi' &= 3m\hat{y}^2 + 3Q_0\hat{x}_\phi(-1 + \Xi), \\ \hat{x}_\varphi' &= -3n\hat{y}^2 + 3Q_0\hat{x}_\varphi(-1 + \Xi), \\ \hat{y}' &= -3\hat{y}(m\hat{x}_\phi + n\hat{x}_\varphi - Q_0\Xi). \end{aligned} \quad (76)$$

Where $\Xi = \hat{x}_\phi^2 - \hat{x}_\varphi^2 + \frac{1}{2}\hat{\Omega}$.

There is also an auxiliary evolution equation

$$\hat{\Omega}' = -Q_0 \left(-2(\hat{x}_\phi^2 - \hat{x}_\varphi^2) + (1 - \hat{\Omega}) \right) \hat{\Omega}. \quad (77)$$

It is useful to express some cosmological parameters in terms of our state variables.⁵

$$(\Omega_m, \Omega_{de}, \Omega_k, q) = \left(\hat{\Omega}, 1 - \hat{\Omega}, Q_0^2 - 1, -1 + 3\Xi \right) / Q_0^2,$$

and

$$w = \frac{\hat{x}_\phi^2 - \hat{x}_\varphi^2 - \hat{y}^2}{\hat{x}_\phi^2 - \hat{x}_\varphi^2 + \hat{y}^2}.$$

3.3.2 Invariance under coordinate transformations.

Observe that the system (76, 77) is invariant under the transformation of coordinates

$$\left(\hat{\tau}, Q_0, \hat{x}_\phi, \hat{x}_\varphi, \hat{y}, \hat{\Omega} \right) \rightarrow \left(-\hat{\tau}, -Q_0, -\hat{x}_\phi, -\hat{x}_\varphi, \hat{y}, \hat{\Omega} \right). \quad (78)$$

Thus, it is sufficient to discuss the behaviour in one part of the phase space, the dynamics in the other part being obtained via the transformation (78). In relation with the possible attractors of the system we will characterize those corresponding to the ‘‘positive’’ branch. The dynamical behavior of the critical points in the ‘‘negative’’ branch is determined by the transformation (78).

3.3.3 Monotonic functions.

The function

$$N = \frac{(n\hat{x}_\phi + m\hat{x}_\varphi)^2 \hat{\Omega}^2}{(1 - Q_0^2)^3}, \quad N' = -6Q_0N \quad (79)$$

is monotonic in the regions $Q_0 < 0$ and $Q_0 > 0$ for $Q_0^2 \neq 1$, $n\hat{x}_\phi + n\hat{x}_\varphi \neq 0$, $\hat{\Omega} > 0$. Hence, there can be no periodic orbits or recurrent orbits in the

⁵We have defined $\Omega_k \equiv \frac{k}{a^2 H^2} = \frac{1}{a^2 H^2}$.

interior of the phase space. Furthermore, it is possible to obtain global results. From the expression N we can immediately see that asymptotically $Q_0^2 \rightarrow 1$ or $n\hat{x}_\phi + m\hat{x}_\varphi \rightarrow 0$ or $\hat{\Omega} \rightarrow 0$.

3.3.4 Local analysis of critical points.

In the tables 7 and 8 it is summarized the location, existence conditions, some properties of the critical points and the eigenvalues of the linearized system around each critical point.

Table 7: Critical points of the system (76). We use the same notation as in table 4.

Label	Coordinates: ($Q_0, \hat{x}_\phi, \hat{x}_\varphi, \hat{y}$)	Existence
$\pm\hat{K}_\pm$	$(\epsilon, \pm\sqrt{1+x_\varphi^{*2}}, x_\varphi^*, 0)$	All m and n
$\pm\hat{F}$	$(\epsilon, 0, 0, 0)$	All m and n
$\pm\hat{S}F$	$(\epsilon, m\epsilon, -n\epsilon, \sqrt{1-\delta})$	$\delta < 1$
$\pm\hat{C}S$	$(\sqrt{3\delta}\epsilon, \frac{m\epsilon}{\sqrt{3\delta}}, -\frac{n\epsilon}{\sqrt{3\delta}}, \sqrt{\frac{2}{3}})$	$0 < \delta < \frac{1}{3}$
$\pm\hat{M}S$	$(\epsilon, \frac{m}{2\delta}, -\frac{n}{2\delta}, \frac{\sqrt{1-\frac{1}{2\delta}}}{2\sqrt{\delta}})$	$\delta > \frac{1}{2}$

In the following we will characterize the dynamical behavior of the cosmological solutions associated with them.

The critical points $\pm\hat{K}_\pm, \pm\hat{F}, \pm\hat{S}F$ and $\pm\hat{M}S$ represents flat FRW solutions.

The set of critical points $\pm\hat{K}_\pm$ parameterised by the real value x_φ^* represents stiff fluid cosmological solutions (DE mimics a stiff fluid). It is the past attractor for ever expanding models provided $n x_\varphi^* \pm m\sqrt{1+x_\varphi^{*2}} < 1$. As we proceed before, a simple application of the symmetry (78), allows to the identification of the future attractor for collapsing models: the typical orbits tends asymptotically to $-\hat{K}_\pm$ as $\hat{\tau} \rightarrow \infty$ provided $n x_\varphi^* \pm m\sqrt{1+x_\varphi^{*2}} > -1$, and $-1 \leq Q_0 < 0$. This fact has interesting consequences. If x_φ^* is a fixed value and n and m are such that $-1 < n x_\varphi^* + m\sqrt{1+x_\varphi^{*2}} < 1$, then, there exists one orbit of the type $+\hat{K}_+ \rightarrow -\hat{K}_+$. If n and m are such that $-1 < n x_\varphi^* - m\sqrt{1+x_\varphi^{*2}} < 1$, then, there is one orbit of the type $+\hat{K}_- \rightarrow -\hat{K}_-$. These are solutions starting from and recollapsing to a singularity given by a MSF cosmology (see figure 6(b)).

The critical points $\pm\hat{F}$ represent flat FRW solutions. They hyperbolic. For these points the scalar fields vanish, so the cosmological parameters associated

Table 8: DE EoS parameter (w), deceleration parameter (q), fractional energy densities, and eigenvalues of the perturbation matrix associated to the critical points of the system (76). We use the notation $\lambda^\pm = nx_\phi^* \pm m\sqrt{1+x_\phi^{*2}}$. When the flow is restricted to the invariant sets $Q_0 = \pm 1$, the eigenvalues associated to the critical points $\pm\hat{F}$, $\pm\hat{SF}$ and $\pm\hat{MS}$ and to the critical sets $\pm\hat{K}_\pm$, are, in each case, the same as those displayed, but the first from the left.

Label	w	q	$\Omega_m, \Omega_{de}, \Omega_k$	Eigenvalues
$\pm\hat{K}_\pm$	1	2	0, 1, 0	$4\epsilon, 0, 3(\epsilon - \lambda^\pm), 3\epsilon$
$\pm\hat{F}$	-	$\frac{1}{2}$	1, 0, 0	$\epsilon, \frac{3}{2}\epsilon, -\frac{3}{2}\epsilon, -\frac{3}{2}\epsilon$
$\pm\hat{SF}$	$-1 + 2\delta$	$-1 + 3\delta$	0, 1, 0	$2(3\delta - 1)\epsilon, 3(\delta - 1)\epsilon, 3(\delta - 1)\epsilon, 3\epsilon$
$\pm\hat{CS}$	$-\frac{1}{3}$	0	$0, \frac{1}{3\delta}, 1 - \frac{1}{3\delta}$	$-2\sqrt{3\delta}\epsilon, -\sqrt{3\delta}\epsilon \pm \sqrt{4 - 9\delta}, -\sqrt{3\delta}\epsilon$
$\pm\hat{MS}$	0	$\frac{1}{2}$	$1 - \frac{1}{2\delta}, \frac{1}{2\delta}, 0$	$\epsilon, -\frac{3}{2}\epsilon, -\frac{3}{4}\left(\epsilon \pm \sqrt{(-7 + \frac{4}{\delta})}\right)\epsilon$

to DE are not applicable to these points. If $\delta > \frac{2}{3}$, the unstable (stable) manifold of $+\hat{F}$ ($-\hat{F}$) is tangent to the critical point and parallel to the plane $\hat{y} - Q_0$. This means that there is an orbit connecting $+\hat{F}$ and $-\hat{F}$ pointing towards $-\hat{F}$ in the direction of the Q_0 -axis. It represents the closed FRW solution with no scalar field starting from a big-bang at $+\hat{F}$ and recollapsing to a “big-crunch” at $-\hat{F}$ (see figure 6(a)).

The critical point $+\hat{SF}$ represents a solution dominated by the scalar field (with non-vanishing potential). It can be the global attractor in the sets $0 < Q_0 < 1$ or $Q_0 = 1$ (i.e., for ever expanding models, or flat models) for the values of the parameters displayed in 9. It can be a phantom dominated solution provided $\delta < 0$. It also can represent quintessence dominated or de Sitter solutions.

The critical point $+\hat{MS}$ exist if $\delta > \frac{1}{2}$. They represent flat matter scaling solutions, for which both the fluid and quintom are dynamically important. It is a saddle point.

For $0 < \delta < \frac{1}{3}$ there exists the critical points $\pm\hat{CS}$ for which the matter is unimportant, but curvature is non-vanishing ($Q_0^2 \neq 1$) and tracks the scalar field. These are called curvature scaling solutions. The values of its cosmological parameters are the same as for $\pm CS$ (displayed in table 5), but it represents a different cosmological solution with positive curvature. These critical points are typically saddle points.

In table 9, where we present a summary of attractors for the quintom model

with $k = 1$.

Table 9: Summary of attractors for the quintom model with $k = 1$ (system (76)). We use the notation $\lambda^\pm = nx_\varphi^* \pm m\sqrt{1 + x_\varphi^{*2}}$.

Restrictions	Past attractor	Future attractor
$Q_0 = -1$	$-\hat{S}F$ if $\delta < \frac{1}{2}$ $-\hat{M}S$ if $\delta > \frac{1}{2}$	$-\hat{K}_\pm$ if $\lambda^\pm > -1$
$-1 < Q_0 < 0$	$-\hat{S}F$ if $\delta < \frac{1}{3}$	as above
$0 < Q_0 < 1$	$+\hat{K}_\pm$ if $\lambda^\pm < 1$	$+\hat{S}F$ if $\delta < \frac{1}{3}$
$Q_0 = 1$	as above	$+\hat{S}F$ if $\delta < \frac{1}{2}$ $+\hat{M}S$ if $\delta > \frac{1}{2}$

3.3.5 Bifurcations.

Observe that the critical points $+\hat{M}S$ y $+\hat{S}F$ coincides as $\delta \rightarrow \frac{1}{2}^+$. $+\hat{C}S$ y $+\hat{S}F$ coincides as $\delta \rightarrow \frac{1}{3}^-$. Additionally, $+\hat{S}F$ ($-\hat{S}F$) coincides with a point at the arc $+\hat{K}_+$ ($-\hat{K}_-$) as $\delta \rightarrow 1^-$. For this values of δ a bifurcation occurs.

3.3.6 Typical behaviour.

Once the attractors have been identified one can give a quantitative description of the physical behaviour of a typical closed quintom cosmology. For example, for ever expanding cosmologies, near the big-bang a typical model behaves like a flat FRW model with stiff fluid represented by the critical set $+\hat{K}_+$ or by $+\hat{K}_-$, depending on the choice of the values of the free parameters m, n and x_φ^* . If $\delta < \frac{1}{3}$ and $0 < Q_0 < 1$ the late time dynamics is determined by $+\hat{S}F$, (with the same physical properties as $+\hat{S}F$). The intermediate dynamics will be governed to a large extent by the fixed points $+\hat{C}S$, $+\hat{M}S$, and $+\hat{F}$, which have the highest lower-dimensional stable manifold. For flat models (i.e., in the invariant set $Q_0 = 1$), the late time dynamics is determined by the critical point $+\hat{S}F$ provided $\delta < \frac{1}{2}$ or $+\hat{M}S$ provided $\delta > \frac{1}{2}$.

For contracting models, the typical behavior is, in one sense, the reverse of the above. If $\delta < \frac{1}{3}$ and $-1 < Q_0 < 0$ the early time dynamics is determined by

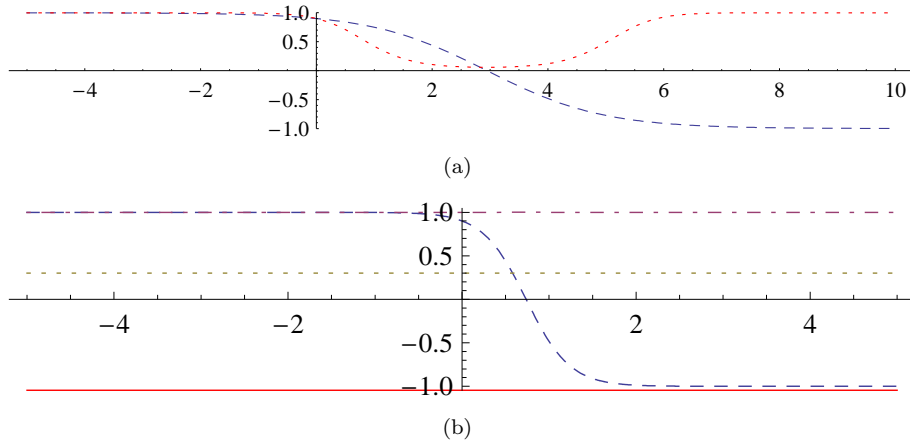


Figure 6: (Color online) *The collapse of quintom cosmologies with positive curvature for the values for the parameters $m = 0.7$, $n = 0.3$ and $\gamma = 1$. In (a) we have selected the initial conditions $Q_0(0) = \hat{\Omega}(0) = 0.9$, and $\hat{x}_\phi(0) = \hat{x}_\varphi(0) = \hat{y}(0) = 0$. The dashed (blue) line represents the evolution of Q_0 vs τ (observe that Q_0 evolves from 1 to -1 , and eventually takes zero value). The dotted (red) line represents $\hat{\Omega}$ vs τ . This illustrates the existence of a closed FRW solution with no scalar field starting from a big-bang at $+\hat{F}$ and recollapsing to a “big-crunch” at $-\hat{F}$. In (b) we have selected the initial conditions $Q_0(0) = 0.9$, $\hat{\Omega}(0) = 0$ and $\hat{x}_\phi(0) = -\sqrt{1 + \hat{x}_\varphi(0)^2}$ with $\hat{x}_\varphi(0) = 0.3$. The dashed (blue) line denotes Q_0 vs τ . Observe that Q_0 goes from the value 1 to -1 (i.e., the model collapses). The dot-dashed line denotes the evolution of $\hat{x}_\phi^2 - x_\phi^2$ vs τ (which is identically equal to 1). The dotted (yellow) line denotes the value of \hat{x}_ϕ vs τ and the straight (red) line denotes the value of x_ϕ vs τ . This illustrates the existence of orbits of the type $+\hat{K}_- \rightarrow -\hat{K}_-$. By choosing $\hat{x}_\phi(0) = \sqrt{1 + \hat{x}_\varphi(0)^2}$, with the same initial conditions for the other variables, we obtain orbits of the type $+\hat{K}_+ \rightarrow -\hat{K}_+$. These are solutions starting from and recollapsing to a singularity (given by a massless scalar field cosmology).*

$_{-}\hat{S}\hat{F}$. The intermediate dynamics will be governed to a large extent by the fixed points $_{-}\hat{C}\hat{S}$, $_{-}\hat{M}\hat{S}$, and $_{-}\hat{F}$, which have the highest lower-dimensional stable manifold. For flat models (i.e., in the invariant set $Q_0 = -1$), the early time dynamics is determined by the critical point $_{-}\hat{S}\hat{F}$ (or $_{-}\hat{M}\hat{F}$) provided $\delta < \frac{1}{2}$ ($\delta > \frac{1}{2}$). A typical model behaves at late times like a flat FRW model with stiff fluid (i.e. the dark energy mimics a stiff fluid) represented by the critical set $_{-}\hat{K}_+$ or by $_{-}\hat{K}_-$ depending on the choice of the values of the free parameters m, n and x_φ^* .

4 Observational Evidence for Quinstant Dark Energy Paradigm

4.1 The model

Looking at the impressive amount of papers addressing the problem of cosmic acceleration clearly shows that two leading candidates to the dark energy throne are the old cosmological constant Λ and a scalar field ϕ evolving under the influence of its self-interaction potential $V(\phi)$.

In the usual approach, one adds either a scalar field or a cosmological constant term to the field equations. However, since what we see is only the final effect of the dark energy components, in principle nothing prevents us to add more than one single component provided that the effective dark energy fluid coming out is able to explain the data at hand. Moreover, as we have hinted upon above, a single scalar field, while explaining cosmic speed up, leads to a problematic eternal acceleration. A possible way out of this problem has been proposed by some of us [38, 39, 92] through the introduction of a negative cosmological term.

Motivated by those encouraging results, we therefore consider a spatially flat universe filled by dust matter, radiation, scalar field and a (negative) cosmological constant term. The Friedmann equations thus read :

$$H^2 = \frac{1}{3} \left[\rho_M + \rho_r + \rho_\Lambda + \frac{1}{2}\dot{\phi}^2 + V(\phi) \right], \quad (80)$$

$$2\dot{H} + 3H^2 = - \left[\frac{1}{3}\rho_r - \rho_\Lambda + \frac{1}{2}\dot{\phi}^2 - V(\phi) \right], \quad (81)$$

where we have used natural units with $8\pi G = c = 1$.

4.2 Matching with the data

Notwithstanding how well motivated it is, a whatever model must be able to reproduce what is observed. This is particularly true for the model we are considering because the presence of a negative cosmological constant introduces a positive pressure term potentially inhibiting the cosmic speed up. Moreover, contrasting the model against the data offers also the possibility to constrain

its characteristic parameters and estimate other derived interesting quantities, such as q_0 , the transition redshift z_T and the age of the universe t_0 . Motivated by these considerations, we will therefore fit our model to the dataset described below parametrizing the model itself with the matter density Ω_M , the scalar field quantities (Ω_ϕ, w_0) and the dimensionless Hubble constant h (i.e., H_0 in units of 100 km/s/Mpc), while we will set the radiation density parameter as $\Omega_r = 10^{-4.3}$ as in [93] from a median of different values reported in literature.

4.2.1 The method and the data

In order to constrain the model parameters we will consider several observational test: (a) the distance modulus $\mu = m - M$, i.e. the difference between the apparent and absolute magnitude of an object at redshift z , (b) the gas mass fraction in galaxy clusters, (c) the measurement of the baryonic acoustic oscillation (BAO) peak in the large scale correlation function at $100 h^{-1}$ Mpc separation detected by Eisenstein et al. [94] using a sample of 46748 luminous red galaxies (LRG) selected from the SDSS Main Sample [95], (d) the shift parameter [96]⁶ and we maximize the following likelihood taking into account the above test:

$$\mathcal{L} \propto \exp \left[-\frac{\chi^2(\mathbf{p})}{2} \right] \quad (82)$$

where $\mathbf{p} = (\Omega_M, \Omega_\phi, w_0, h)$ denotes the set of model parameters and the pseudo- χ^2 merit function reads:

$$\begin{aligned} \chi^2(\mathbf{p}) &= \sum_{i=1}^N \left[\frac{\mu^{th}(z_i, \mathbf{p}) - \mu_i^{obs}}{\sigma_i} \right]^2 + \sum_{i=1}^N \left[\frac{f_{gas}^{th}(z_i, \mathbf{p}) - f_{gas,i}^{obs}}{\sigma_i} \right]^2 \\ &+ \left[\frac{\mathcal{A}(\mathbf{p}) - 0.474}{0.017} \right]^2 + \left[\frac{\mathcal{R}(\mathbf{p}) - 1.70}{0.03} \right]^2 + \left(\frac{h - 0.72}{0.08} \right)^2. \quad (83) \end{aligned}$$

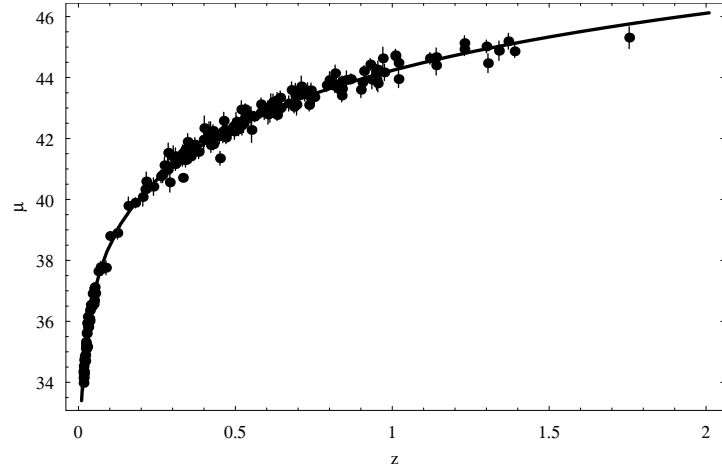
4.2.2 Results

Table 1 shows the best fit model parameters, median values and 1 and 2σ ranges for the parameters $(\Omega_M, \Omega_\Lambda, w_0, h, \Omega_\phi)$.

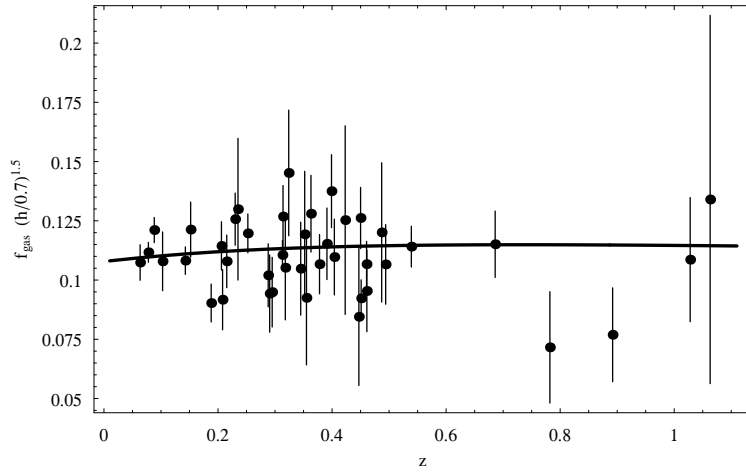
Figs.7 shows how well our best fit model reproduce the data on the SNeIa Hubble diagram and gas mass fraction. The best fit model is in quite good agreement with both the SNeIa and gas data. Actually, the χ^2 values are respectively 206 and 48 to be contrasted with the number of datapoints, being 192 and 42 respectively. Besides the predicted values for the acoustic peak and shift parameters are in satisfactory agreement with the observed ones:

$$\mathcal{A} = 0.45 \quad , \quad \mathcal{R} = 1.67. \quad (84)$$

⁶a complete discussion about this observational test and the quinstant model can be found in [39]



(a)



(b)

Figure 7: (Color online) (a) Best fit curve superimposed to the data on the SNeIa Hubble diagram. (b) Best fit curve superimposed to the data on the gas mass fraction. Note that the theoretical curve plots indeed $f_{\text{gas}}(z) \times (h/0.7)^{1.5}$ with h set to its best fit value (from [39]).

Table 10: Best fit (*bf*) and median (*med*) values and 1σ and 2σ ranges of the parameters $(\Omega_M, \Omega_\Lambda, w_0, h, \Omega_\phi)$ as obtained from the likelihood analysis (from [39]).

Par	<i>bf</i>	<i>med</i>	1σ	2σ
Ω_M	0.283	0.307	(0.272, 0.352)	(0.246, 0.410)
Ω_Λ	-0.072	-0.298	(-0.54, -0.11)	(-0.92, -0.02)
w_0	-0.72	-0.67	(-0.74, -0.60)	(-0.79, -0.53)
h	0.632	0.620	(0.588, 0.654)	(0.554, 0.692)
Ω_ϕ	0.789	0.989	(0.799, 1.226)	(0.700, 1.574)

Because of these results, we can therefore conclude that including a negative Λ leads to a model still in agreement with the data so that this approach to halting eternal acceleration is a viable one from an observational point of view.
7

Another interesting tools to study the viability of a dark energy model is the point of view of structure formation. This kind of analysis can break between models with similar prediction from the cosmic expansion history, in this sense the growth of the large scale structure in the universe provide and important companion test. Following this line in [97] the authors showed that the quinstant model makes reasonable predictions for the formation of linear large scale structure of the Universe but it fails in the non linear regime because of the density contrast at virialisation increase with the value of virialisation redshif.

Concerning the predictions of the cluster abundances, the quinstant model is capable of reproducing the results of the other models in a satisfactory way backwards in time up to redshifts a bit larger than $z = 1$ for the three range of mass values ⁸. Then, it shows abrupt peaks of structure formation, in a serious departure of the hierarchical model for large scale structure. This seems to be caused by the unusual equation of state of quinstant dark energy, which behaves as stiff matter for redshifts a bit larger than one. This would result in enhanced accretion of the forming structures, both because of gravitational and viscous forces.

5 Exponential Quinstant: Phase space analysis

In this section we will investigate, from the dynamical systems viewpoint the quinstant dark energy model with exponential potential $V(\phi) = V_0 e^{\lambda\phi}$. We do not consider radiation fluid here but a background of a perfect fluid with equation of state $w = \gamma - 1$. The cosmological equations reads:

⁷see [39] for a further discussion about the observational results and implications

⁸the same behavior is obtained for other mass range [97]

$$H^2 - \frac{1}{6}\dot{\phi}^2 - \frac{1}{3}V(\phi) - \frac{1}{3}\rho_M - \frac{\Lambda}{3} = -\frac{k}{a^2}, \quad k = -1, 0, 1, \quad (85)$$

$$\dot{H} = -H^2 - \frac{1}{3}\dot{\phi}^2 + \frac{1}{3}V(\phi) + \frac{\Lambda}{3} - \frac{1}{6}(3\gamma - 2)\rho_M, \quad (86)$$

$$\dot{\rho}_M = -3\gamma H\rho_M, \quad (87)$$

$$\ddot{\phi} + 3H\dot{\phi} + \frac{dV(\phi)}{d\phi} = 0. \quad (88)$$

Our purpose is to re-express the former equations as an autonomous dynamical system.

5.1 Flat FRW case

5.1.1 Normalization, state space, and dynamical system.

In order to get a first order autonomous system of ordinary differential equations (ODEs) it is convenient to introduce normalized variables and a new convenient (monotonic) time variable. If the phase space is compact the flow of the system admits both past and future attractors. Let us introduce the normalization factor $D = \sqrt{H^2 - \Lambda/3} > 0$, the new time variable $d\tau = Ddt$, and the phase space variables:

$$x = \frac{\dot{\phi}}{\sqrt{6}D}, \quad y = \frac{\sqrt{V(\phi)}}{\sqrt{3}D}, \quad \mathcal{H} = \frac{H}{D}. \quad (89)$$

The former variables lie in the compact phase space

$$\{(x, y, z) : x^2 + y^2 \leq 1, y \geq 0, -1 \leq \mathcal{H} \leq 1\}.$$

The variables (89) satisfy the ODEs (the prime denoting derivative with respect to τ):

$$\begin{aligned} x' &= -\frac{3}{2}x\mathcal{H}((\gamma - 2)x^2 + (y^2 - 1)\gamma + 2) \\ &\quad - \sqrt{\frac{3}{2}}\lambda y^2, \end{aligned} \quad (90)$$

$$y' = \frac{3}{2}y \left(\frac{\sqrt{6}\lambda x}{3} - \mathcal{H}((\gamma - 2)x^2 + (y^2 - 1)\gamma) \right), \quad (91)$$

$$\mathcal{H}' = -\frac{3}{2}(\mathcal{H}^2 - 1)((\gamma - 2)x^2 + (y^2 - 1)\gamma) \quad (92)$$

For convenience, let us express some cosmological quantities in terms of the variables (89). The deceleration parameter is explicitly

$$q \equiv -\ddot{a}a/\dot{a}^2 = -1 + \frac{3}{2} \left[\frac{x^2(2 - \gamma) + (1 - y^2)\gamma}{\mathcal{H}^2} \right]; \quad (93)$$

the fractional energy density of the scalar field is

$$\Omega_\phi = \frac{x^2 + y^2}{\mathcal{H}^2}; \quad (94)$$

and the 'effective' EoS parameter is given by

$$\omega_{eff} \equiv \frac{P_{tot}}{\rho_{tot}} \equiv \frac{\frac{1}{2}\dot{\phi}^2 - V(\phi) + (\gamma - 1)\rho_M - \Lambda}{\frac{1}{2}\dot{\phi}^2 + V(\phi) + \rho_M + \Lambda} = -1 + \frac{(2 - \gamma)x^2 + (1 - y^2)\gamma}{\mathcal{H}^2}. \quad (95)$$

5.1.2 Form invariance under coordinate transformations.

The system (90-92) is form invariant under the coordinate transformation and time reversal

$$(\tau, x, y, \mathcal{H}) \rightarrow (-\tau, -x, y, -\mathcal{H}). \quad (96)$$

Thus, it is sufficient to discuss the behaviour in one part of the phase space, the dynamics in the other part being obtained via the transformation (96). Observe also, that equations (90-92) are form invariant under the coordinate transformation $y \rightarrow -y$. Then, (90-92) is form invariant under its composition with (96).

From equation (92) follows that $\mathcal{H} = \pm 1$ are invariant sets of the flow. From equation (91) follows that the sign of y is invariant.

5.1.3 Monotonic functions.

Let be defined

$$Z(x, y, \mathcal{H}) = \left(\frac{\mathcal{H} + 1}{\mathcal{H} - 1} \right)^2 \quad (97)$$

in the invariant set

$$S = \{(x, y, \mathcal{H}) : x^2 + y^2 < 1, y > 0, -1 < \mathcal{H} < 1\}.$$

Then, Z is monotonic decreasing in S since

$$Z' \equiv \nabla Z \cdot f = -6Z(x^2(2 - \gamma) + (1 - y^2)\gamma) < 0$$

in S . The existence of this monotonic allows to state that there can be no periodic orbits or recurrent orbits in the interior of the phase space. Furthermore, it is possible to obtain global results. The range of Z is the semi-interval $(0, +\infty)$, and $Z \rightarrow 0$ as $\mathcal{H} \rightarrow -1$ (since \mathcal{H} is bounded) and $Z \rightarrow +\infty$ as $\mathcal{H} \rightarrow 1$. By applying the Monotonicity Principle (theorem 4.12 [91]) we find that, for all $p \in S$, the past asymptotic attractor of p (the α -limit) belongs to $\mathcal{H} = 1$ and the future asymptotic attractor of p (the ω -limit) belongs to $\mathcal{H} = -1$.

5.1.4 Local analysis of critical points.

The system (90-91) admits ten critical points with the labels P_i^\pm with $i = 1 \dots 5$. In table 11 we offer some partial information about the location, conditions for existence and some additional properties of them. All the critical points satisfy

$\mathcal{H} = \pm 1$. In other words, they are solutions with $H = \pm D$ (i.e. with $H \rightarrow \pm\infty$). If $\text{sign}(\mathcal{H}) = -1$ the associated solutions ends in a collapse (since $H < 0$), whereas, if $\text{sign}(\mathcal{H}) = 1$ we have ever expanding cosmological solutions. The expected cosmological behavior of our model is that the attractor solutions represent collapsing solutions due the negative value of the cosmological constant.

Table 11: Location and existence conditions of the critical points of the system (90-92)

Label	Coordinates: (x, y, \mathcal{H})	Existence
P_1^\pm	$(-1, 0, \pm 1)$	All λ
P_2^\pm	$(0, 0, \pm 1)$	All λ
P_3^\pm	$(1, 0, \pm 1)$	All λ
P_4^\pm	$\left(\mp \frac{\lambda}{\sqrt{6}}, \sqrt{1 - \frac{\lambda^2}{6}}, \pm 1\right)$	$-\sqrt{6} < \lambda < \sqrt{6}$
P_5^\pm	$\left(\mp \sqrt{\frac{3}{2}} \frac{\gamma}{\lambda}, \sqrt{\frac{3}{2}} \sqrt{\frac{(2-\gamma)\gamma}{\lambda^2}}, \pm 1\right)$	$\gamma = 0, \lambda \neq 0$ $0 < \gamma \leq 2, \lambda \geq \sqrt{3}\gamma$

Now, let us make some comments about the cosmological solutions associated to these critical points.

The critical points P_1^\pm and P_3^\pm represent stiff-matter solutions which are associated with massless scalar field cosmologies (the kinetic energy density of the scalar field dominated against the potential energy density). In the former case the scalar field is a monotonic decreasing function of t (since its time-derivative is negative). In the last case the scalar field is an increasing function of t since its time-derivative is positive. These solutions are always decelerated. The critical points P_2^\pm represent a flat FRW solution fuelled by perfect fluid. They represent accelerating solutions for $\gamma < \frac{2}{3}$. The critical points P_4^\pm represent solutions dominated by the scalar field ($\Omega_\phi = 1$, and $H \rightarrow \pm\infty$) which are accelerating if $\lambda^2 < 2$. Our models does not devoid of scaling phases: the critical points P_5^\pm are such that neither the scalar field nor the perfect fluid dominates the evolution. There $\Omega_m/\Omega_\phi = \text{const.}$, and $\gamma_\phi = \gamma$.

Before proceed to make some numerical experiments let us discuss some aspects concerning the symmetry (96). Observe that the critical points $P_3^\mp, P_2^\mp, P_4^\mp$ and P_5^\mp are related by the transformation (96) with $P_1^\pm, P_2^\pm, P_4^\pm$ and P_5^\pm respectively. In order to analyze the local stability of $P_1^+, P_2^+, P_3^+, P_4^+, P_5^+$ it is sufficient analyse the local stability of $P_3^-, P_2^-, P_1^-, P_4^-, P_5^-$ respectively, and then, infer the stability of the points in the ‘‘positive’’ branch by using (96).

Table 12: Eigenvalues, and dynamical character of the fixed points of (90-92). We use the notation $\Delta = (2 - \gamma)(24\gamma^2 + \lambda^2(2 - 9\gamma))$.

Label	Eigenvalues	Dynamical character
P_1^-	$-6, -3 - \sqrt{\frac{3}{2}}\lambda, -3(2 - \gamma)$	nonhyperbolic if $\gamma = 2$ or $\lambda = -\sqrt{6}$; stable (node) if $\lambda > -\sqrt{6}$ and $\gamma \neq 2$; saddle, otherwise.
P_2^-	$\frac{3}{2}(2 - \gamma), -3\gamma, -\frac{3\gamma}{2}$	nonhyperbolic if $\gamma = 0$ or $\gamma = 2$; saddle, otherwise.
P_3^-	$-6, -3 + \sqrt{\frac{3}{2}}\lambda, -3(2 - \gamma)$	nonhyperbolic if $\gamma = 2$ or $\lambda = \sqrt{6}$; stable (node) if $\lambda < \sqrt{6}$ and $\gamma \neq 2$; saddle, otherwise.
P_4^-	$-\lambda^2, \frac{1}{2}(6 - \lambda^2), -\lambda^2 + 3\gamma$	nonhyperbolic if $\lambda = 0$ or $\lambda^2 = 3\gamma$; saddle, otherwise.
P_5^-	$-3\gamma, \frac{3}{4}\left(2 - \gamma \pm \frac{1}{\lambda}\sqrt{\Delta}\right)$	nonhyperbolic if $\gamma = 0$ or $\lambda^2 = 3\gamma$; saddle, otherwise.

In table 12 we offer partial information about the dynamical character of the critical points corresponding to the “negative” branch.

The critical point P_1^- is nonhyperbolic provided $\gamma = 2$ or $\lambda = -\sqrt{6}$. It is a stable node (future attractor) provided $\lambda > -\sqrt{6}$ and $\gamma \neq 2$. It is a saddle otherwise with a 2D stable manifold and a 1D unstable manifold tangent to the y -axis. P_2^- is nonhyperbolic provided $\gamma = 0$ or $\gamma = 2$. It is a saddle point otherwise with a 2D stable manifold and a 1D unstable manifold tangent to the x -axis. The critical point P_3^- is nonhyperbolic provided $\gamma = 2$ or $\lambda = \sqrt{6}$. It is a stable node (future attractor) provided $\lambda < \sqrt{6}$ and $\gamma \neq 2$. It is a saddle otherwise with a 2D stable manifold and a 1D unstable manifold tangent to the y -axis. P_4^- is nonhyperbolic if $\lambda^2 \in \{0, 3\gamma, 6\}$. Saddle otherwise, with a 2D stable manifold provided $\lambda^2 > 3\gamma$ or 1D if $\lambda^2 < 3\gamma$. The critical point P_5^- is nonhyperbolic if $\gamma = 0$ or $\lambda^2 = 3\gamma$. It is a saddle point, otherwise, with a 2D unstable manifold provided $0 < \gamma < 2$ and $\lambda^2 > 3\gamma$. P_4^- (P_5^-) is the past attractor in the invariant set $\mathcal{H} = -1$ provided $0 < \gamma < 2$, $\lambda^2 < 3\gamma$ ($0 < \gamma < 2$, $\lambda^2 > 3\gamma$).

In table 14, where we present a summary of attractors (both past and future) for the quinstant model with $k = 0$.

In figure 8 we show some orbits in the phase space for the values $\lambda = -\sqrt{\frac{3}{2}}$ and $\gamma = 1$. For this choice $\lambda^2 < 3\gamma$ and $-\sqrt{6} < \lambda < \sqrt{6}$. Thus the critical points P_5^\pm do not exist. By the linear analysis (see table 12) we find that the critical

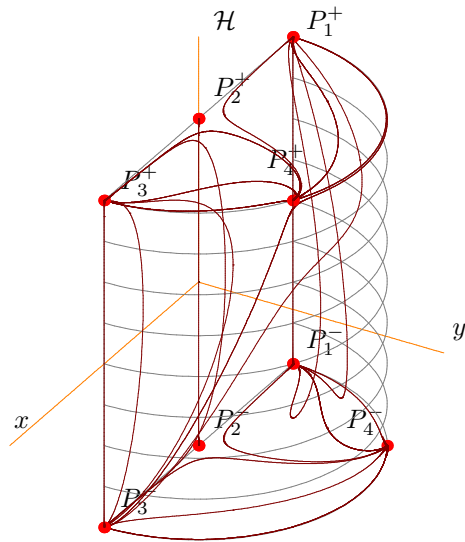


Figure 8: (Color online) *Some orbits of (90-91) in the phase space for the values $\lambda = -\sqrt{\frac{3}{2}}$ and $\gamma = 1$. The critical points P_1^- (resp. P_1^+) and P_3^- (resp. P_3^+) are the future (resp. past) asymptotic attractors, P_3^- (resp. P_1^+) having a stronger attracting (resp. unstable) manifold tangent to the y -axis. P_4^+ , acts as a local attractor in the invariant set $\mathcal{H} = 1$ and P_4^- , acts as the local source for the invariant set $\mathcal{H} = -1$ (they are, however, saddle points for the 3D dynamics).*

Table 13: Some properties of the critical points of the system (90-92)

Label	Deceleration q	Ω_ϕ	ω_{eff}
P_1^\pm	2	1	1
P_2^\pm	$-1 + \frac{3\gamma}{2}$	0	$-1 + \gamma$
P_3^\pm	2	1	1
P_4^\pm	$-1 + \frac{\lambda^2}{2}$	1	$-1 + \frac{\lambda^2}{3}$
P_5^\pm	$-1 + \frac{3\gamma}{2}$	$\frac{3\gamma}{\lambda^2}$	$-1 + \gamma$

 Table 14: Summary of attractors for for the quinstant model with $k = 0$ (system (90-92)).

Restrictions	Past attractor	Future attractor
$\mathcal{H} = -1$	P_4^- if $0 < \gamma < 2, \lambda^2 < 3\gamma$	P_3^- if $\lambda < \sqrt{6}, \gamma \neq 2$
	P_5^- if $0 < \gamma < 2, \lambda^2 > 3\gamma$	P_1^- if $\lambda > -\sqrt{6}, \gamma \neq 2$
$-1 < \mathcal{H} < 1$	P_3^+ if $\lambda > -\sqrt{6}, \gamma \neq 2$	as above
	P_1^+ if $\lambda < \sqrt{6}, \gamma \neq 2$	
$\mathcal{H} = 1$	as above	P_4^+ if $0 < \gamma < 2, \lambda^2 < 3\gamma$
		P_5^+ if $0 < \gamma < 2, \lambda^2 > 3\gamma$

points P_1^- and P_3^- have a 3-dimensional stable manifold, P_3^- having a stronger attracting manifold tangent to the y -axis (see figure 8), i.e., two global future attractors might coexist (bistability). The critical points P_1^+ and P_3^+ are local sources in the invariant set $\mathcal{H} = 1$. Numerical inspection suggest and analytical results confirm that they are also global sources, P_1^+ having a stronger unstable direction tangent to y -axis. The critical points P_2^\pm acts locally as saddles. For P_2^- (resp. P_2^+) the stable (resp. unstable) manifold is 2-dimensional and tangent to the y - \mathcal{H} plane. There are orbits (corresponding to exact cosmological solutions) connecting $P_{1,2,3}^+$ with $P_{1,2,3}^-$ (recollapse occurs). The critical point P_4^+ , with coordinates $(1/2, \sqrt{3}/2, 1)$, have eigenvalues $-2.25, -1.5, 1.5$ act-

ing as a local attractor in the invariant set $\mathcal{H} = 1$ and P_4^- , with coordinates $(-1/2, \sqrt{3}/2, 1)$, and eigenvalues $2.25, 1.5, -1.5$ is the local source for the invariant set $\mathcal{H} = -1$. They are saddle points for the 3D dynamics (see figure 8).

5.1.5 Bifurcations.

The critical points (P_4^+, P_4^-) reduce to (P_1^+, P_3^-) as $\lambda \rightarrow (\sqrt{6})^-$. The critical points (P_4^+, P_4^-) reduce to (P_3^+, P_1^-) as $\lambda \rightarrow (-\sqrt{6})^+$. The critical points P_5^\pm reduce to P_2^\pm as $\gamma \rightarrow 0^+$. On the other hand, P_5^\pm reduce to P_4^\pm as $\lambda \rightarrow (\sqrt{3\gamma})^+$ or $\lambda \rightarrow (-\sqrt{3\gamma})^-$. For these values of the parameters a bifurcation arises.

5.1.6 Typical behavior

Once the attractors have been identified one can give a quantitative description of the physical behavior of a typical flat quinstant cosmology.

For example, for ever expanding cosmologies with $H > 0, H \rightarrow +\infty, \mathcal{H} = 1$, i.e., the standard expanding cosmology near the big-bang, a typical model behaves like a massless scalar field (kinetic dominated energy density) represented by P_3^+ or P_1^+ provided $\lambda > -\sqrt{6}, \gamma \neq 2$ or $\lambda < \sqrt{6}, \gamma \neq 2$, respectively. This types of solutions might coexist in the same phase space. The late time dynamics in $\mathcal{H} = 1$ is given by either a scalar field dominated solution ($\Omega_\phi \rightarrow 1$) represented by P_4^+ or by a scaling solution ($\Omega_m/\Omega_\phi = O(1)$) represented by P_5^+ provided $\lambda^2 < 3\gamma$ or $\lambda^2 > 3\gamma$, respectively. For finite values of H , i.e., $-1 < \mathcal{H} < 1$, the early time dynamics is the same as in the previous case but there are subtle differences with respect the late time dynamics. In fact, in the invariant set $-1 < \mathcal{H} < 1$ the future attractors are P_3^- or P_1^- depending if $\lambda < \sqrt{6}, \gamma \neq 2$ or $\lambda > -\sqrt{6}, \gamma \neq 2$. If $|\lambda| < \sqrt{6}$ the system is bistable. Such solutions represent contracting stiff-fluid cosmologies. This means that a typical quinstant cosmologies allows the collapse of matter when the time evolves. For contracting cosmologies with $(H < 0, H \rightarrow \infty, \mathcal{H} = -1)$, i.e., the standard contracting model near the initial singularity, the late time dynamics is the same as int the previously described case, i.e., the collapse. However, there are subtle differences concerning the early time dynamics. The late time dynamics in $\mathcal{H} = -1$ is given by either a scalar field dominated solution ($\Omega_\phi \rightarrow 1$) represented by P_4^- or by a scaling solution ($\Omega_m/\Omega_\phi = O(1)$) represented by P_5^- provided $\lambda^2 < 3\gamma$ or $\lambda^2 > 3\gamma$.

5.2 Quinstant cosmology with negative curvature

5.2.1 Normalization, state space, and dynamical system.

Let us consider the same normalization as in section 5.1.1, i.e, the normalization factor $D = \sqrt{H^2 - \Lambda/3} > 0$ and the time variable $d\tau = Ddt$. We will consider the variables (89) augmented by the new variable $z = \frac{1}{aD}$. These variables lies

in the compact phase space

$$\{(x, y, z, \mathcal{H}) : x^2 + y^2 + z^2 \leq 1, y \geq 0, z \geq 0, -1 \leq \mathcal{H} \leq 1\}.$$

The variables x , y , z , and \mathcal{H} satisfy the ASODE (the prime denoting derivative with respect to τ):

$$\begin{aligned} x' &= -\frac{3}{2}x\mathcal{H} \left((\gamma - 2)x^2 + (y^2 - 1)\gamma + z^2 \left(\gamma - \frac{2}{3} \right) + 2 \right) \\ &\quad - \sqrt{\frac{3}{2}}\lambda y^2, \end{aligned} \quad (98)$$

$$y' = \frac{3}{2}y \left(\frac{\sqrt{6}\lambda x}{3} - \mathcal{H} \left((\gamma - 2)x^2 + (y^2 - 1)\gamma + z^2 \left(\gamma - \frac{2}{3} \right) \right) \right), \quad (99)$$

$$z' = \frac{3}{2}z\mathcal{H} \left((\gamma - 2)x^2 + (y^2 - 1)\gamma + z^2 \left(\gamma - \frac{2}{3} \right) - \frac{2}{3} \right) \quad (100)$$

$$\mathcal{H}' = -\frac{3}{2}(\mathcal{H}^2 - 1) \left((\gamma - 2)x^2 + (y^2 - 1)\gamma + z^2 \left(\gamma - \frac{2}{3} \right) \right) \quad (101)$$

As before, we will re-express the cosmological magnitudes of interest in terms of the normalized variables.

The deceleration parameter is explicitly

$$q \equiv -\ddot{a}/\dot{a}^2 = -1 + \frac{3}{2} \left[\frac{x^2(2-\gamma) + (1-y^2)\gamma + z^2(\frac{2}{3}-\gamma)}{\mathcal{H}^2} \right]; \quad (102)$$

the fractional energy density of the scalar field and curvature are given respectively by

$$\Omega_\phi = \frac{x^2 + y^2}{\mathcal{H}^2}; \Omega_k = \frac{z^2}{\mathcal{H}^2} \quad (103)$$

and the 'effective' EoS parameter is given by

$$\omega_{eff} \equiv \frac{P_{tot}}{\rho_{tot}} \equiv \frac{\frac{1}{2}\dot{\phi}^2 - V(\phi) + (\gamma - 1)\rho_M - \Lambda}{\frac{1}{2}\dot{\phi}^2 + V(\phi) + \rho_M + \Lambda} = -1 + \frac{(2-\gamma)x^2 + (1-y^2)\gamma - \gamma z^2}{\mathcal{H}^2 - z^2}. \quad (104)$$

5.2.2 Form invariance under coordinate transformations.

The system (98-101) is form invariant under the coordinate transformation and time reversal

$$(\tau, x, y, z, \mathcal{H}) \rightarrow (-\tau, -x, y, z, -\mathcal{H}). \quad (105)$$

Thus, it is sufficient to discuss the behaviour in one part of the phase space, the dynamics in the other part being obtained via the transformation (105).

Observe that equations (98-101) are form invariant under the coordinate transformation $y \rightarrow -y$ and $z \rightarrow -z$. Then, (98-101) is form invariant under they composition with (105).

There are four obvious invariant sets under the flow of (98-101), they are $y = 0$, $z = 0$, and $\mathcal{H} = \pm 1$. They combination defines other invariant sets. The dynamics restricted to the invariant set $z = 0$ is the same described in section 5.1. It is of course of interest the analysis of the behavior of the 4D orbits near the invariant set $z = 0$ (or the other enumerated above). We will discuss this in next sections.

5.2.3 Monotonic functions.

Let be defined

$$Z_1 = \left(\frac{\mathcal{H} + 1}{\mathcal{H} - 1} \right)^2 \quad (106)$$

in the invariant set

$$\{(x, y, z, \mathcal{H}) : x^2 + y^2 + z^2 < 1, y > 0, z > 0, -1 < \mathcal{H} < 1\}.$$

Then, Z is monotonic decreasing in S since

$$Z' \equiv \nabla Z \cdot f = -Z (4z^2 + 6x^2 (2 - \gamma) + 6 (1 - y^2 - z^2) \gamma) < 0$$

in S . The range of Z is the semi-interval $(0, +\infty)$, and $Z \rightarrow 0$ as $\mathcal{H} \rightarrow -1$ (since \mathcal{H} is bounded) and $Z \rightarrow +\infty$ as $\mathcal{H} \rightarrow 1$. By applying the Monotonicity Principle (theorem 4.12 [91]) we find that, for all $p \in S$, the past asymptotic attractor of p (the α -limit) belongs to $\mathcal{H} = 1$ and the future asymptotic attractor of p (the ω -limit) belongs to $\mathcal{H} = -1$.

Let be defined in the same invariant set the function

$$Z_2 = \frac{z^4}{(1 - x^2 - y^2 - z^2)^2}, \quad Z_2' = -2(2 - 3\gamma) \mathcal{H} Z_2 \quad (107)$$

This function is monotonic in the regions $\mathcal{H} < 0$ and $\mathcal{H} > 0$ for $\gamma \neq \frac{2}{3}$.

The existence of monotonic functions allows to state that there can be no periodic orbits or recurrent orbits in the interior of the phase space. Furthermore, it is possible to obtain global results. From the expression Z_2 we can immediately see that asymptotically $z \rightarrow 0$ or $x^2 + y^2 + z^2 \rightarrow 1$.

5.2.4 Local analysis of critical points.

The system (98-101) admits fourteen critical points. We will denote the critical points of the system (98-101) located at the invariant set $z = 0$ in the same way as in the table 11 of section 5.1.4. We submit the reader to this table for the conditions for their existence. In table 17 are summarized the stability properties of the critical points.

Observe that the critical points P_6^\mp and P_7^\pm are related through (105) with the critical points P_6^\pm and P_7^\mp respectively.

In order to analyze the local stability of $P_1^+, P_2^+, P_3^+, P_4^+, P_5^+, P_6^+, P_7^+$ it is sufficient analyze the local stability of $P_3^-, P_2^-, P_1^-, P_4^-, P_5^-, P_6^-, P_7^-$ respectively, and then, infer the stability of the points in the “positive” branch by using (105). In table 17 we offer a detailed analysis of the dynamical character of the critical points corresponding to the “negative” branch.

The critical point P_1^- is nonhyperbolic if $\gamma = 2$ or $\lambda = -\sqrt{6}$. It is a local sink provided $\lambda > -\sqrt{6}, \gamma \neq 0$. If $\lambda < -\sqrt{6}$ then there exists a 1D unstable manifold tangent to the \hat{y} -axis, and a 3D stable manifold. The critical point P_2^- is nonhyperbolic if $\gamma = 0, \gamma = \frac{2}{3}$ or $\gamma = 2$. There exist always at least a 1D unstable manifold tangent to the x axis. The unstable manifold is 2D provided $\gamma < \frac{2}{3}$. In this case there exists a 2D stable manifold tangent to the $y\text{-}\mathcal{H}$ plane. The critical point P_3^- is nonhyperbolic if $\gamma = 2$ or $\lambda = \sqrt{6}$. It is a local sink provided $\lambda < \sqrt{6}, \gamma \neq 0$. If $\lambda > \sqrt{6}$ then there exists a 1D unstable manifold tangent to the y -axis, and a 3D stable manifold. Observe that P_1^- and P_3^- coexist provided $\lambda^2 < 6$. In this case both are the future attractors of the system, they attract solutions in its basin of attraction. The critical point P_4^- is hyperbolic if $\lambda \in \{0, \pm 3\gamma, \pm 2\}$. If not, it is always a saddle point with an unstable manifold at least 1D. The stable manifold is 3D provided $0 < \gamma \leq \frac{2}{3}, 2 < \lambda^2 < 6$ or $\frac{2}{3} < \gamma < 2, 3\gamma < \lambda^2 < 6$. It is 2D provided $0 < \gamma < \frac{2}{3}, 3\gamma < \lambda^2 < 2$ or $\frac{2}{3} < \gamma < 2, 2 < \lambda^2 < 3\gamma$ or 1D provided $0 < \gamma \leq \frac{2}{3}, 0 < \lambda^2 < 3\gamma$ or $\frac{2}{3} < \gamma < 2, 0 < \lambda^2 < 2$. The critical point P_5^- is nonhyperbolic if $\gamma = 0$ or $\lambda^2 = 3\gamma$ or $\gamma = \frac{2}{3}$. If not, it have always two conjugate complex eigenvalues with positive real parts (there exists at least a 2D unstable manifold). The stable manifold is 1D provided $0 < \gamma \leq \frac{2}{9}, \lambda^2 > 3\gamma$ or $\frac{2}{9} < \gamma < \frac{2}{3}, \lambda^2 < \frac{24\gamma^2}{-2+9\gamma}$ or 2D if $\frac{2}{3} < \gamma < 2, \lambda^2 < \frac{24\gamma^2}{-2+9\gamma}$. Thus, P_5^- is always a saddle point.

In the negative curvature case there are two new classes of critical points: Mine’s solutions and curvature-scaling solutions, denoted by P_6^\pm and P_7^\pm respectively. In table 15 it is displayed the location, existence and some properties of them.

Table 15: Location and existence conditions of the critical points P_6^\pm and P_7^\pm of the system (98-101).

Label	Coordinates: (x, y, z, \mathcal{H})	Existence
P_6^\pm	$(0, 0, 1, \pm 1)$	All λ
P_7^\pm	$(\mp \frac{1}{\lambda} \sqrt{\frac{2}{3}}, \frac{2}{\sqrt{3}\lambda}, \frac{1}{\lambda} \sqrt{-2 + \lambda^2}, \pm 1)$	$\frac{2}{3} < \gamma \leq 2$ and $ \lambda \geq \sqrt{2}$

In table 18, where we present a summary of attractors (both past and future) for the quinstant model with $k = -1$.

Table 16: Some properties of the critical points P_6^\pm and P_7^\pm of the system (98-101).

Label	Deceleration q	Ω_ϕ	ω_{eff}
P_6^\pm	0	1	0
P_7^\pm	$\frac{2}{\lambda^2}$	$1 - \frac{2}{\lambda^2}$	$-\frac{1}{3}$

In figure 9 are displayed typical orbits of the system (98-101) in the invariant set $\mathcal{H} = 1$ for the values $\lambda = -\sqrt{\frac{3}{2}}$ and $\gamma = 1$. The critical points P_1^+ and P_3^+ are the past asymptotic attractors, P_1^+ having a stronger unstable manifold tangent to the y -axis. P_4^+ , acts as a local attractor in the invariant set $\mathcal{H} = 1$. The Milne's universe (P_6^+) is the local future attractor in the invariant set $y = 0$. In figure 10 are drawn some orbits in the invariant set $\mathcal{H} = -\infty$ for the same choice. The critical points P_1^- and P_3^- are the future asymptotic attractors, P_3^- having a stronger attracting manifold tangent to the y -axis. P_4^- acts as the local source for the invariant set $z = 0$ (they are, however, saddle points for the 4D dynamics). The Milne's universe (P_6^-) is the local past attractor in the invariant set $y = 0$. This is the better we can do numerically since the phase space is actually 4D.

5.2.5 Bifurcations.

The critical points (P_4^+, P_4^-) reduce to (P_1^+, P_3^-) as $\lambda \rightarrow (\sqrt{6})^-$. The critical points (P_4^+, P_4^-) reduce to (P_3^+, P_1^-) as $\lambda \rightarrow (-\sqrt{6})^+$. The critical points P_5^\pm reduce to P_2^\pm as $\gamma \rightarrow 0^+$. On the other hand, P_5^\pm reduce to P_4^\pm as $\lambda \rightarrow (\sqrt{3\gamma})^+$ or $\lambda \rightarrow (-\sqrt{3\gamma})^-$. The critical points P_7^\pm , P_5^\pm and P_4^\pm coincide as $\gamma \rightarrow (\frac{2}{3})^+$ and $\lambda \rightarrow (\sqrt{2})^+$ simultaneously. For these values of the parameters a bifurcation arises.

5.2.6 Typical behavior.

Once the attractors have been identified one can give a quantitative description of the physical behavior of a typical negatively curved quinstant cosmology.

For example, for ever expanding cosmologies with $H > 0, H \rightarrow +\infty, \mathcal{H} = 1$, i.e., the standard expanding cosmology near the big-bang, a typical model behaves like a massless scalar field (kinetic dominated energy density) represented by P_3^+ or P_1^+ provided $\lambda > -\sqrt{6}, \gamma \neq 2$ or $\lambda < \sqrt{6}, \gamma \neq 2$, respectively. This types of solutions might coexist in the same phase space. The late time dynamics in $\mathcal{H} = 1$ is given by either a scalar field dominated solution ($\Omega_\phi \rightarrow 1$) represented by P_4^+ provided $0 < \gamma < 2, \lambda^2 < 3\gamma$ or $\frac{2}{3} < \gamma \leq 2, \lambda^2 < 2$; or by a

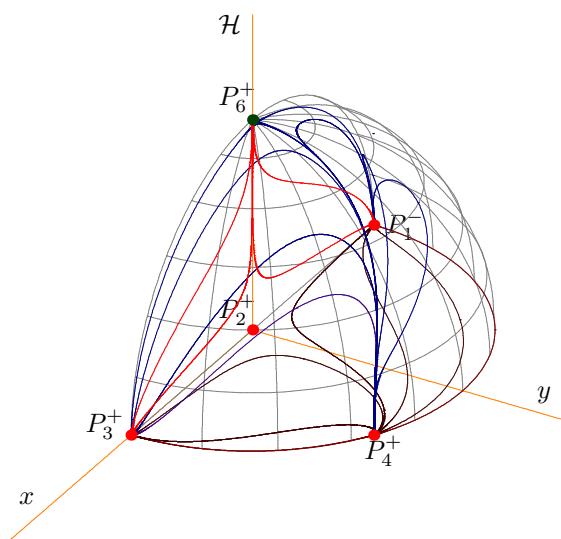


Figure 9: (Color online) *Some orbits of (98-101) in the invariant set $\mathcal{H} = 1$ for the values $\lambda = -\sqrt{\frac{3}{2}}$ and $\gamma = 1$.*

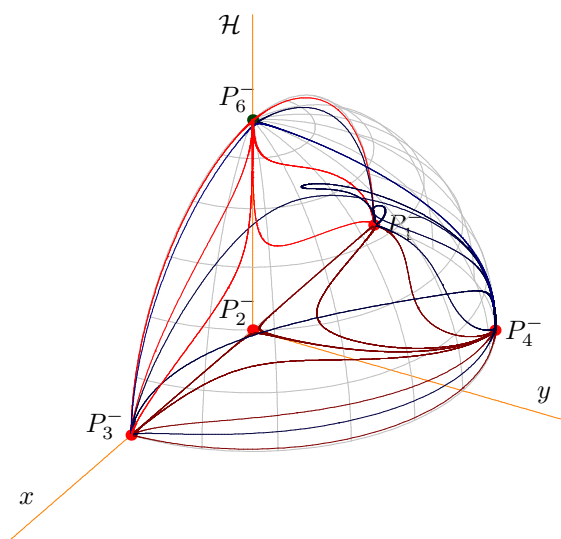


Figure 10: (Color online) *Some orbits of (98-101) in the invariant set $\mathcal{H} = -1$ for the values $\lambda = -\sqrt{\frac{3}{2}}$ and $\gamma = 1$.*

Table 17: Eigenvalues, and dynamical character of the fixed points of the system (98-101). We use the notation $\Delta = (2 - \gamma)(24\gamma^2 + \lambda^2(2 - 9\gamma))$.

Label	Eigenvalues	Dynamical character
P_1^-	$-6, -3 - \sqrt{\frac{3}{2}}\lambda, -3(2 - \gamma), -2$	nonhyperbolic if $\gamma = 2$ or $\lambda = -\sqrt{6}$; stable (node) if $\lambda > -\sqrt{6}$ and $\gamma \neq 2$; saddle, otherwise.
P_2^-	$\frac{3}{2}(2 - \gamma), -3\gamma, -\frac{3\gamma}{2}, 1 - \frac{3\gamma}{2}$	nonhyperbolic if $\gamma = 0$ or $\gamma = 2$ or $\gamma = \frac{2}{3}$; saddle, otherwise.
P_3^-	$-6, -3 + \sqrt{\frac{3}{2}}\lambda, -3(2 - \gamma), -2$	nonhyperbolic if $\gamma = 2$ or $\lambda = \sqrt{6}$; stable (node) if $\lambda < \sqrt{6}$ and $\gamma \neq 2$; saddle, otherwise.
P_4^-	$-\lambda^2, \frac{1}{2}(6 - \lambda^2), -\lambda^2 + 3\gamma, 1 - \frac{\lambda^2}{2}$	nonhyperbolic if $\lambda = 0$ or $\lambda^2 = 3\gamma$; saddle, otherwise.
P_5^-	$-3\gamma, \frac{3}{4}\left(2 - \gamma \pm \frac{1}{\lambda}\sqrt{\Delta}\right), 1 - \frac{3\gamma}{2}$	nonhyperbolic if $\gamma = 0$ or $\lambda^2 = 3\gamma$ or $\gamma = \frac{2}{3}$; saddle, otherwise.
P_6^-	$-2, 2, -1, -2 + 3\gamma$	nonhyperbolic if $\gamma = \frac{2}{3}$; saddle, otherwise.
P_7^-	$-2, 1 \pm \sqrt{\frac{8}{\lambda^2} - 3}, -2 + 3\gamma$	nonhyperbolic if $\lambda^2 = 2$ or $\gamma = \frac{2}{3}$; unstable, otherwise.

scaling solution ($\Omega_m/\Omega_\phi = O(1)$) represented by P_5^+ for $0 < \gamma < \frac{2}{3}, \lambda^2 > 2$; or by a curvature scaling solution represented by P_7^+ provided $\frac{2}{3} < \gamma \leq 2, \lambda^2 > 2$. For finite values of H , i.e., $-1 < \mathcal{H} < 1$, the early time dynamics is the same as in the previous case but there are subtle differences with respect the late time dynamics. In fact, in the invariant set $-1 < \mathcal{H} < 1$ the future attractors are P_3^- or P_1^- depending if $\lambda < \sqrt{6}, \gamma \neq 2$ or $\lambda > -\sqrt{6}, \gamma \neq 2$. If $|\lambda| < \sqrt{6}$ the system is bistable. Such solutions represent contracting stiff-fluid cosmologies. This means that a typical quinstant negatively curved cosmologies allows the collapse of matter when the time evolves. For contracting cosmologies with ($H < 0, H \rightarrow \infty, \mathcal{H} = -1$), i.e., the standard contracting model near the initial singularity, the late time dynamics is the same as in the previously described case, i.e., the collapse. However, there are subtle differences concerning the early time dynamics. The late time dynamics in $\mathcal{H} = -1$ is given by either a scalar field dominated solution ($\Omega_\phi \rightarrow 1$) represented by P_4^- provided $0 < \gamma < 2, \lambda^2 < 3\gamma$ or $\frac{2}{3} < \gamma \leq 2, \lambda^2 < 2$; or by a scaling solution ($\Omega_m/\Omega_\phi = O(1)$) represented by P_5^- for $0 < \gamma < \frac{2}{3}, \lambda^2 > 2$; or by a curvature

Table 18: Summary of attractors for for the quinstant model with $k = -1$ (system (98-101)).

Restrictions	Past attractor	Future attractor
$\mathcal{H} = -1$	P_4^- if $0 < \gamma < 2, \lambda^2 < 3\gamma$ or if $\frac{2}{3} < \gamma \leq 2, \lambda^2 < 2$ P_5^- if $0 < \gamma < \frac{2}{3}, \lambda^2 > 3\gamma$ P_7^- if $\frac{2}{3} < \gamma \leq 2, \lambda^2 > 2$	P_3^- if $\lambda < \sqrt{6}, \gamma \neq 2$ P_1^- if $\lambda > -\sqrt{6}, \gamma \neq 2$
$-1 < \mathcal{H} < 1$	P_3^+ if $\lambda > -\sqrt{6}, \gamma \neq 2$ P_1^+ if $\lambda < \sqrt{6}, \gamma \neq 2$	as above
$\mathcal{H} = 1$	as above	P_4^+ if $0 < \gamma < 2, \lambda^2 < 3\gamma$ or if $\frac{2}{3} < \gamma \leq 2, \lambda^2 < 2$ P_5^+ if $0 < \gamma < \frac{2}{3}, \lambda^2 > 3\gamma$ P_7^+ if $\frac{2}{3} < \gamma \leq 2, \lambda^2 > 2$

scaling solution represented by P_7^- provided $\frac{2}{3} < \gamma \leq 2, \lambda^2 > 2$.

5.3 Quinstant cosmology with positive curvature

5.3.1 Normalization, state space, and dynamical system.

Let us consider the normalization factor $\hat{D} = \sqrt{H^2 - \Lambda/3 + \frac{1}{a^2}} > 0$ and the time variable $d\hat{\tau} = \hat{D}dt$, and the phase space variables:

$$\hat{x} = \frac{\dot{\phi}}{\sqrt{6}\hat{D}}, \hat{y} = \frac{\sqrt{V(\phi)}}{\sqrt{3}\hat{D}}, \hat{H} = \frac{H}{\hat{D}}, \hat{z} = \frac{1}{a\hat{D}}. \quad (108)$$

The former variables lies in the compact phase space

$$\left\{ (x, y, z) : x^2 + y^2 \leq 1, y \geq 0, -1 \leq \hat{H} \leq 1, 0 \leq z \leq 1 \right\}.$$

The variables $\hat{x}, \hat{y}, \hat{z}$, and \hat{H} satisfy the ASODE (the prime denoting derivative with respect to $\hat{\tau}$):

$$\hat{x}' = \frac{3}{2}\hat{x}\hat{H}((2-\gamma)(1-\hat{x}^2) - \gamma\hat{y}^2) - \frac{\sqrt{6}}{2}\lambda\hat{y}^2, \quad (109)$$

$$\hat{y}' = \frac{3}{2}\hat{y}\hat{H}((2-\gamma)\hat{x}^2 + \gamma(1-\hat{y}^2)) + \frac{\sqrt{6}}{2}\lambda\hat{x}\hat{y}, \quad (110)$$

$$\hat{z}' = \frac{1}{2}\hat{z}\hat{H}(3(2-\gamma)\hat{x}^2 + 3\gamma(1-\hat{y}^2) - 2) \quad (111)$$

$$\hat{H}' = -\frac{3}{2}(\hat{H}^2 - 1)((\gamma - 2)\hat{x}^2 + (\hat{y}^2 - 1)\gamma) + \hat{z}^2 \quad (112)$$

As before, we will re-express the cosmological magnitudes of interest in terms of the normalized variables.

The deceleration parameter is explicitly

$$q \equiv -\ddot{a}a/\dot{a}^2 = -1 + \frac{3}{2} \left[\frac{\hat{x}^2(2-\gamma) + (1-\hat{y}^2)\gamma}{\hat{H}^2} \right] - \frac{\hat{z}^2}{\hat{H}^2}; \quad (113)$$

the fractional energy density of the scalar field and curvature are given respectively by

$$\Omega_\phi = \frac{\hat{x}^2 + \hat{y}^2}{\hat{H}^2}; \Omega_k = \frac{\hat{z}^2}{\hat{H}^2} \quad (114)$$

and the 'effective' EoS parameter is given by

$$\omega_{eff} \equiv \frac{P_{tot}}{\rho_{tot}} \equiv \frac{\frac{1}{2}\dot{\phi}^2 - V(\phi) + (\gamma - 1)\rho_M - \Lambda}{\frac{1}{2}\dot{\phi}^2 + V(\phi) + \rho_M + \Lambda} = -1 + \frac{(2-\gamma)\hat{x}^2 + (1-\hat{y}^2)\gamma}{\hat{H}^2 + \hat{z}^2}. \quad (115)$$

5.3.2 Form invariance under coordinate transformations.

The system (109-112) is form invariant under the coordinate transformation and time reversal

$$(\hat{\tau}, \hat{x}, \hat{y}, \hat{z}, \hat{H}) \rightarrow (-\hat{\tau}, -\hat{x}, \hat{y}, \hat{z}, -\hat{H}). \quad (116)$$

Thus, it is sufficient to discuss the behavior in one part of the phase space, the dynamics in the other part being obtained via the transformation (116). Observe that equations (109-112) are form invariant under the coordinate transformation $\hat{y} \rightarrow -\hat{y}$ and $\hat{z} \rightarrow -\hat{z}$. Then, (109-112) is form invariant under they composition with (116).

There are two obvious invariant sets under the flow of (109-112), they are $\hat{y} = 0, \hat{z} = 0$.

From equation (112) we can immediately see that the surfaces $\hat{H} = \pm 1$ are not invariant provided $z \neq 0$. In fact, the surfaces $\hat{H} = \pm 1$ act as membranes (that can be crossed). This follows from the fact that $H'|_{H=\pm 1} = z^2 > 0$ for $z \neq 0$. Observe that if initially $z > 0$, then, from equation (111), follows that the sign of z is invariant. Only if $z = 0$, the surfaces $\hat{H} = \pm 1$ could be invariant.

5.3.3 Monotonic functions

Let be defined in the invariant set

$$\left\{(\hat{x}, \hat{y}, \hat{z}, \hat{H}) : \hat{x}^2 + \hat{y}^2 < 1, \hat{y} > 0, 0 < z < 1, -1 < \hat{H} < 1\right\},$$

the function

$$Z = \frac{z^4}{(1 - x^2 - y^2)^2}, \quad Z' = -2(2 - 3\gamma) \hat{H}Z \quad (117)$$

This function is monotonic in the regions $\hat{H} < 0$ and $\hat{H} > 0$ for $\gamma \neq \frac{2}{3}$.

The existence of this monotonic function allows to state that there can be no periodic orbits or recurrent orbits in the interior of the phase space. Furthermore, it is possible to obtain global results. From the expression Z we can immediately see that asymptotically $z \rightarrow 0$ or $x^2 + y^2 \rightarrow 1$.

5.3.4 Local analysis of critical points.

Table 19: Location and existence conditions of the critical points of the system (109-111)

Label	Coordinates: $(\hat{x}, \hat{y}, \hat{z}, \hat{H})$	Existence
\hat{P}_1^\pm	$(-1, 0, 0, \pm 1)$	All λ
\hat{P}_2^\pm	$(0, 0, 0, \pm 1)$	All λ
\hat{P}_3^\pm	$(1, 0, 0, \pm 1)$	All λ
\hat{P}_4^\pm	$\left(\mp \frac{\lambda}{\sqrt{6}}, \sqrt{1 - \frac{\lambda^2}{6}}, 0, \pm 1\right)$	$-\sqrt{6} < \lambda < \sqrt{6}$
\hat{P}_5^\pm	$\left(\mp \sqrt{\frac{3}{2}} \frac{\gamma}{\lambda}, \sqrt{\frac{3}{2}} \sqrt{\frac{(2-\gamma)\gamma}{\lambda^2}}, 0, \pm 1\right)$	$\gamma = 0, \lambda \neq 0$ $0 < \gamma \leq 2, \lambda \geq \sqrt{3\gamma}$
\hat{P}_6	$\left(x^*, 0, \sqrt{\frac{3}{2}(\gamma + (2-\gamma)x^{*2})}, 0\right)$	$0 \leq \gamma \leq \frac{2}{3}, x^* \leq \sqrt{\frac{2-3\gamma}{3(2-\gamma)}}$
\hat{P}_7^\pm	$\left(\mp \frac{1}{\sqrt{3}}, \sqrt{\frac{2}{3}}, \sqrt{1 - \frac{\lambda^2}{2}}, \pm \frac{\lambda}{\sqrt{2}}\right)$	$-\sqrt{2} \leq \lambda \leq \sqrt{2}$

Table 20: Eigenvalues, and dynamical character of the fixed points of the system (98-101). We use the notation $\Delta = (2 - \gamma)(24\gamma^2 + \lambda^2(2 - 9\gamma))$ and $\mu = \sqrt{\frac{3}{2}((x^*)^2 - 1)\gamma(2 - 3\gamma) + 24x^*^2}$.

Label	Eigenvalues	Dynamical character
\hat{P}_1^-	$-6, -3 - \sqrt{\frac{3}{2}}\lambda, -3(2 - \gamma), -2$	nonhyperbolic if $\gamma = 2$ or $\lambda = -\sqrt{6}$; stable (node) if $\lambda > -\sqrt{6}$ and $\gamma \neq 2$; saddle, otherwise.
\hat{P}_2^-	$\frac{3}{2}(2 - \gamma), -3\gamma, -\frac{3\gamma}{2}, 1 - \frac{3\gamma}{2}$	nonhyperbolic if $\gamma = 0$ or $\gamma = 2$ or $\gamma = \frac{2}{3}$; saddle otherwise.
\hat{P}_3^-	$-6, -3 + \sqrt{\frac{3}{2}}\lambda, -3(2 - \gamma), -2$	nonhyperbolic if $\gamma = 2$ or $\lambda = \sqrt{6}$; stable (node) if $\lambda < \sqrt{6}$ and $\gamma \neq 2$; saddle, otherwise.
\hat{P}_4^-	$-\lambda^2, \frac{1}{2}(6 - \lambda^2), -\lambda^2 + 3\gamma, 1 - \frac{\lambda^2}{2}$	nonhyperbolic if $\lambda = 0$ or $\lambda^2 = 3\gamma$ or $\lambda^2 = 2$; saddle otherwise.
\hat{P}_5^-	$-3\gamma, \frac{3}{4}\left(2 - \gamma \pm \frac{1}{\lambda}\sqrt{\Delta}\right), 1 - \frac{3\gamma}{2}$	nonhyperbolic if $\gamma = 0$ or $\lambda^2 = 3\gamma$ or $\gamma = \frac{2}{3}$; saddle, otherwise.
\hat{P}_6	$0, \sqrt{\frac{3}{2}}\lambda x^*, -\mu, \mu$	nonhyperbolic
\hat{P}_7^-	$-\sqrt{2}\lambda, \frac{\lambda \pm \sqrt{8 - 3\lambda^2}}{\sqrt{2}}, \frac{(3\gamma - 2)\lambda}{\sqrt{2}}$	nonhyperbolic if $\lambda = 0$ or $\lambda^2 = 2$; or $\gamma = \frac{2}{3}$; unstable (saddle), otherwise.

Using (116), it is possible to infer the local stability of $\hat{P}_1^+, \hat{P}_2^+, \hat{P}_3^+, \hat{P}_4^+, \hat{P}_5^+, \hat{P}_7^+$ from the local stability of $\hat{P}_3^-, \hat{P}_2^-, \hat{P}_1^-, \hat{P}_4^-, \hat{P}_5^-, \hat{P}_7^-$. Thus, we will analyze only the critical points in the “negative” branch.

The critical points \hat{P}_1^+ to \hat{P}_5^+ have similar properties, dynamical character as unhatted ones in section 5.2 and the same physical interpretation of the unhatted ones characterized in section 5.1. Thus, we will not comment about its stability in detail. For completeness in table 20 are summarize the existence conditions and stability properties. We will submit the interested reader to previous sections for more details.

For the positive curvature model there are new critical points: the curve of nonhyperbolic critical points \hat{P}_6 represent the Einstein’s static universe. Special critical points of this family are those with the choice $x^* = 0$ (it exists provided $0 \leq \gamma \leq \frac{2}{3}$) and $x^* = \pm \sqrt{\frac{3(2-3\gamma)}{2-\gamma}}$ (it exists provided $0 \leq \gamma < \frac{2}{3}$), and the curvature-scaling solution \hat{P}_7^\pm . Concerning the stability of curvature-scaling solutions we have that \hat{P}_7^- is always a saddle point (at least one eigenvalues has

negative real part, and the others are of different sign). Its stable manifold is 1D provided $-\sqrt{2} < \lambda < 0$, $0 < \gamma < \frac{2}{3}$; or 2D provided $0 < \lambda < \sqrt{2}$, $\frac{2}{3} < \gamma < 2$ or $-\sqrt{2} < \lambda < 0$, $\frac{2}{3} < \gamma < 2$; or 3D if $0 < \lambda < \sqrt{2}$, $0 \leq \gamma < \frac{2}{3}$.

5.3.5 Bifurcations.

The critical points $(\hat{P}_4^+, \hat{P}_4^-)$ reduce to $(\hat{P}_1^+, \hat{P}_3^-)$ as $\lambda \rightarrow (\sqrt{6})^-$. The critical points $(\hat{P}_4^+, \hat{P}_4^-)$ reduce to $(\hat{P}_3^+, \hat{P}_1^-)$ as $\lambda \rightarrow (-\sqrt{6})^+$. The critical points \hat{P}_5^\pm reduce to \hat{P}_2^\pm as $\gamma \rightarrow 0^+$. On the other hand, \hat{P}_5^\pm reduce to \hat{P}_4^\pm as $\lambda \rightarrow (\sqrt{3\gamma})^+$ or $\lambda \rightarrow (-\sqrt{3\gamma})^-$. $(\hat{P}_7^+, \hat{P}_7^-)$ reduce to $(\hat{P}_4^+, \hat{P}_4^-)$ as $\lambda \rightarrow (\sqrt{2})^-$ and $(\hat{P}_7^+, \hat{P}_7^-)$ reduce to $(\hat{P}_4^-, \hat{P}_4^+)$ as $\lambda \rightarrow (-\sqrt{2})^+$. For these values of the parameters a bifurcation arises.

5.3.6 Typical behavior.

As a consequence that $\hat{H} = \pm 1$ are not invariant sets, the determination of past and future attractors is more simpler. If $\lambda < -\sqrt{6}$, $\gamma \neq 2$, then P_1^+ is the past attractor and P_3^- is the future attractor. If $-\sqrt{6} < \lambda < \sqrt{6}$, $\gamma \neq 2$ the past attractors are both \hat{P}_3^+ and \hat{P}_1^+ and the future attractors are both \hat{P}_1^- and \hat{P}_3^- . Finally, if $\lambda > \sqrt{6}$, $\gamma \neq 2$ then P_3^+ is the past attractor and P_1^- is the future attractor. In any case the Universe evolves from a stiff regime to a stiff regime by crossing the value $\hat{H} = 0$, allowing the collapse of the Universe.

In table 21, where we present a summary of attractors (both past and future) for the quinstant model with $k = 1$.

Table 21: Summary of attractors for for the quinstant model with $k = 1$ (system (109-112)) for $z > 0$.

Past attractor	Future attractor
\hat{P}_3^+ if $\lambda > -\sqrt{6}$, $\gamma \neq 2$	\hat{P}_3^- if $\lambda < \sqrt{6}$, $\gamma \neq 2$
\hat{P}_1^+ if $\lambda < \sqrt{6}$, $\gamma \neq 2$	\hat{P}_1^- if $\lambda > -\sqrt{6}$, $\gamma \neq 2$

6 Observational Test and Dynamical Systems: The Interplay

Dynamical systems techniques by one way and Observational test by the other are strongly enough to discriminate among the wide variety of dark energy models nowadays under investigation. The first one is more mathematical in

character: they can be used to select the better behaved models, with appropriate attractors in the past and future. These tools to analyse and interpreted results has gained a lot of attention in recent years. The techniques are so powerful when we want to investigate the asymptotic (and even, intermediate) behavior of models. The other class of tools is rather physical: they can be used of astrophysical observations to crack the degeneracy of classes of dark energy models. In the interplay, both serve to constraint the free parameters of the models under consideration. In our case, quintom and quinstant dark energy, with flat and curved geometry.

Quintom Dark Energy Paradigm

The model of quintom, which is mainly favored by current SNIa only, needs to be confronted with other observations in the framework of concordance cosmology. Since SNIa offer the only direct detection of DE, this model is the most promising to be distinguished from the cosmological constant and other dynamical DE models which do not get across -1 , by future SNIa projects on the low redshift (for illustrations see e.g. [44]).

From the dynamical systems viewpoint we have obtained further results in support of the previous results in [12, 13, 16]. For negative curvature models, we have devised two dynamical systems adapted to the study of expanding ($\epsilon = \text{sign } H > 0$) and contracting ($\epsilon = \text{sign } H < 0$) models. Also, we have devised another dynamical system well suited for investigating positive curvature models. We have characterized the critical points of each system and interpreted the cosmological solutions associated. By devising well defined monotonic functions we were able to get global results for ever expanding and contracting models (for both negative and positive curvature models). We have reviewed the results concerning the flat case. It is known that, for flat ever expanding models the attractor will be the matter scaling solution [16]. If matter scaling solutions do not exist, the attractor will be phantom ($w < -1$) or de Sitter ($w = -1$) like. This is a difference with respect to the results in [12] and [13]. It was proved there, that the attractor solutions are de Sitter-like, unless some trajectories cross, transiently, the $w = -1$ boundary to become even smaller before ending in a de Sitter phase.

The new results we survey here are as follows:

For negative-curvature ever-expanding models ($\epsilon = \text{sign } H > 0$) we have obtained the existence of scaling curvature attractors (without matter) (provided $\delta < \frac{1}{3}$). The attractor solution will be dominated by DE whenever its existence precludes the existence of scaling curvature attractors. These solutions can be: phantom-like ($w < -1$), de Sitter-like ($w = -1$), or quintessence-like. This is a difference with respect the situation in [16]. We must notice, however, that if we consider other values for γ , other than $\gamma = 1$, then the attractor of the system can be the matter scaling solution. This is the case if $0 < \gamma < \frac{2}{3}$, $\delta > \frac{\gamma}{2}$. Under the above conditions on the parameters DM mimics DE. For contracting models ($\epsilon = \text{sign } H < 0$), the attractor will be a MSF solution that mimics a stiff fluid. Towards the past, the typical situation is the reverse of the former

described. For positive curvature (closed) models, we have obtained conditions under which there is an orbit of type $+\hat{K} \rightarrow -\hat{K}$. This represents a cosmological solution starting in a ending towards a singularity describe a MSF cosmology. We have obtained, also, a flat FRW solution starting in a big-bang in $+F$ y recolapsing in a “big-crunch” in $-F$. We have illustrated this results by means of numerical integrations of the ASODE describing this cosmological model. We have obtained conditions for the existence of global attractors. We have offered, here, only a simplified qualitative analysis (as a difference of the mathematical analysis in [88] pages 69-73). However, our study have relevance by its own right, and can be considered in some way as a complement of the former since we have added a phantom field in the dynamics. We must to restate, however, that our analysis is not as detailed as in that reference. But its is suffice to illustrated our goals. The qualitative analysis in multi- scalar field (coventional) cosmologies with exponential potentials (in the context of assisted inflation) was done in the same reference, section VII, and in [89, 90], particularly for two fields. They do not consider phantom field as we do here. Our monotonic functions were able to discard the existence of periodic orbits, homoclinic orbits, or recurrent orbits.

Quinstant Dark Energy Paradigm

From the stability analysis of all studied models of (exponential) quinstant dark energy ([38], [39]), the typical behavior, irrespective the curvature choice, is the evolution from an stiff-regime near the past, to a stiff-regime in the far future. Besides, from our dynamical analysis it seems that for negatively curvature and flat models, the model shows the divergence of the Hubble parameter (H) in the asymptotic regimes. There are other cosmological models of composite dark energy having stiff-matter domination as an attractor in the past, but usually they would not be global attractors, but local. This is the case of several models of quintom dark energy. From the structure formation we see that QDE makes reasonable predictions for the formation of linear large scale structure of the Universe. It reproduces reasonably well the non-linear structures from today up to redshifts a bit larger than one, but fails to reproduce the perturbations in the non-linear regime for redshifts a bit larger than one. This models are dynamically equivalent models of $f(R)$ modified gravity. It would be interesting to study how these $f(R)$ models behave concerning structure formation, and then we would have a better understanding on how these observations would crack the degeneracy dark energy- $f(R)$ modified gravity.

In summary, the new results concerning quinstant dark energy are as follows:

For the standard flat expanding cosmology near the big-bang, a typical model behaves like a massless scalar field (kinetic dominated energy density) and the late time dynamics is given by either a scalar field dominated solution ($\Omega_\phi \rightarrow 1$) or by a scaling solution ($\Omega_m/\Omega_\phi = O(1)$) represented by P_5^+ provided $\lambda^2 < 3\gamma$. This is the standard behavior for quintessence models (without Λ). For finite values of H , the early time dynamics is the same as in the previous case but there are subtle differences with respect the late time dynamics. In fact, in this invariant set the future attractors are stiff-like (contracting) solutions with

$H \rightarrow \pm\infty$. This means that a typical quinstant cosmologies allows the collapse of matter when the time evolves. For the standard contracting model near the initial singularity, the late time and early time dynamics is the reverse of the previously described.

The behavior of a typical negatively curved quinstant model is similar to the flat situation, but not the same. The differences is in that in the limit $H \rightarrow \infty$ the late time dynamics given by either a scalar field dominated solution ($\Omega_\phi \rightarrow 1$) provided $0 < \gamma < 2, \lambda^2 < 3\gamma$ or $\frac{2}{3} < \gamma \leq 2, \lambda^2 < 2$; or by a scaling solution ($\Omega_m/\Omega_\phi = O(1)$) for $0 < \gamma < \frac{2}{3}, \lambda^2 > 2$; or by a curvature scaling solution provided $\frac{2}{3} < \gamma \leq 2, \lambda^2 > 2$. For finite values of H , the future attractors are stiff-like solutions. For positive curvature models the Universe evolves from a stiff regime to a stiff regime by crossing the value $\dot{H} = 0$, allowing the collapse of the Universe. Thus, from the dynamical view point there are not significant differences between quinstant and quintom dark energy paradigms.

Our opinion is that any dark energy model which presents a stiff-like equation of state in the past, during a long period of time, will predict abrupt peaks of structure formation, which would be the result of enhanced accretion of the forming structures, both because of gravitational and viscous forces.

References

- [1] E. J. Copeland, M. Sami, and S. Tsujikawa, *Int. J. Mod. Phys.* **D15** (2006) 1753–1936.
- [2] R. R. Caldwell and M. Kamionkowski, arXiv:0903.0866 [astro-ph.CO].
- [3] S. M. Carroll, W. H. Press, and E. L. Turner, *Ann. Rev. Astron. Astrophys.* **30** (1992) 499–542.
- [4] V. Sahni and A. A. Starobinsky, *Int. J. Mod. Phys.* **D9** (2000) 373–444.
- [5] T. Padmanabhan, *Phys. Rept.* **380** (2003) 235–320.
- [6] V. Sahni, *Class. Quant. Grav.* **19**, 3435 (2002) [arXiv:astro-ph/0202076].
- [7] Feng B., Wang X. L. and Zhang X. M., 2005, *Phys. Lett. B* **607**, 35 [arXiv:astro-ph/0404224].
- [8] Wei H. and Cai R. G., 2006, *Phys. Lett. B* **634**, 9 [arXiv:astro-ph/0512018].
- [9] Sadjadi H. M. and Alimohammadi M., 2006, *Phys. Rev. D* **74**, 043506 [arXiv:gr-qc/0605143].
- [10] M. R. Setare and E. N. Saridakis, *JCAP* **0809**, 026 (2008) [arXiv:0809.0114 [hep-th]].
- [11] M. R. Setare and E. N. Saridakis, *Phys. Rev. D* **79**, 043005 (2009) [arXiv:0810.4775 [astro-ph]].

- [12] Guo Z. K., Piao Y. S., Zhang X. M. and Zhang Y. Z., 2005, Phys. Lett. B **608**, 177 [arXiv:astro-ph/0410654].
- [13] Zhang X. F., Li H., Piao Y. S. and Zhang X. M., 2006, Mod. Phys. Lett. A **21**, 231 [arXiv:astro-ph/0501652].
- [14] Wei H. and Cai R. G., 2005, Phys. Rev. D **72**, 123507 [arXiv:astro-ph/0509328].
- [15] Wei H., Cai R. G. and Zeng D. F., 2005, Class. Quant. Grav. **22**, 3189 [arXiv:hep-th/0501160].
- [16] Lazkoz R. and Leon G., 2006, Phys. Lett. B **638**, 303 [arXiv:astro-ph/0602590].
- [17] Zhang X., Int. J. Mod. Phys. D **14**, 1597 [arXiv:astro-ph/0504586].
- [18] Zhang X. and Wu F. Q., Phys. Rev. D **72**, 043524 [arXiv:astro-ph/0506310].
- [19] Zhang X., Phys. Rev. D **74**, 103505 [arXiv:astro-ph/0609699].
- [20] E. N. Saridakis, Phys. Lett. B **661**, 335 (2008) [arXiv:0712.3806 [gr-qc]].
- [21] M. R. Setare and E. N. Saridakis, Phys. Lett. B **671**, 331 (2009) [arXiv:0810.0645 [hep-th]].
- [22] Y. f. Cai, M. z. Li, J. X. Lu, Y. S. Piao, T. t. Qiu and X. m. Zhang, Phys. Lett. B **651**, 1 (2007) [arXiv:hep-th/0701016].
- [23] Zhang S. and Chen B., arXiv:0806.4435 [hep-ph].
- [24] Sadeghi J., Setare M. R., Banijamali A. and Milani F., 2008, Phys. Lett. B **662**, 92 [arXiv:0804.0553 [hep-th]].
- [25] Cai Y. F. and Wang J., 2008, Class. Quant. Grav. **25**, 165014 [arXiv:0806.3890 [hep-th]].
- [26] E. N. Saridakis, P. F. Gonzalez-Diaz and C. L. Siguenza, Class. Quant. Grav. **26**, 165003 (2009) [arXiv:0901.1213 [astro-ph]].
- [27] Lazkoz R., Leon G. and Quiros I., 2007, Phys. Lett. B **649**, 103 [arXiv:astro-ph/0701353].
- [28] Alimohammadi M. and Sadjadi H. M., 2007, Phys. Lett. B **648**, 113 [arXiv:gr-qc/0608016].
- [29] Alimohammadi M., 2008, Gen. Rel. Grav. **40**, 107 [arXiv:0706.1360 [gr-qc]].
- [30] M. R. Setare and E. N. Saridakis, Int. J. Mod. Phys. D **18**, 549 (2009) [arXiv:0807.3807 [hep-th]].
- [31] M. R. Setare and E. N. Saridakis, Phys. Lett. B **668**, 177 (2008) [arXiv:0802.2595 [hep-th]].

- [32] E. Elizalde, S. Nojiri and S. D. Odintsov, *Phys. Rev. D* **70**, 043539 (2004) [arXiv:hep-th/0405034].
- [33] P. S. Apostolopoulos and N. Tetradis, *Phys. Rev. D* **74**, 064021 (2006) [arXiv:hep-th/0604014].
- [34] K. Bamba, S. Nojiri and S. D. Odintsov, *Phys. Rev. D* **77**, 123532 (2008) [arXiv:0803.3384 [hep-th]].
- [35] K. Bamba, C. Q. Geng, S. Nojiri and S. D. Odintsov, *Phys. Rev. D* **79**, 083014 (2009) [arXiv:0810.4296 [hep-th]].
- [36] M. R. Setare and E. N. Saridakis, *JCAP* **0903**, 002 (2009) [arXiv:0811.4253 [hep-th]].
- [37] S. Nojiri and S. D. Odintsov, eConf **C0602061**, 06 (2006) [*Int. J. Geom. Meth. Mod. Phys.* **4**, 115 (2007)] [arXiv:hep-th/0601213].
- [38] R. Cardenas, T. Gonzalez, Y. Leyva, O. Martin, and I. Quiros, *Phys. Rev. D* **67** (2003) 083501.
- [39] V. F. Cardone, R. P. Cardenas, and Y. Leyva Nodal, *Class. Quant. Grav.* **25** (2008) 135010.
- [40] J. Grande, J. Sola and H. Stefancic, *AIP Conf. Proc.* **878**, 220 (2006) [arXiv:astro-ph/0609683].
- [41] J. Grande, J. Sola and H. Stefancic, *Phys. Lett. B* **645**, 236 (2007) [arXiv:gr-qc/0609083].
- [42] J. Grande, J. Sola and H. Stefancic, *JCAP* **0608**, 011 (2006) [arXiv:gr-qc/0604057].
- [43] J. Grande, J. Sola and H. Stefancic, *J. Phys. A* **40**, 6787 (2007) [arXiv:gr-qc/0701090].
- [44] D. Huterer and A. Cooray, *Phys. Rev. D* **71**, 023506 (2005) [arXiv:astro-ph/0404062].
- [45] D. Huterer and G. Starkman, *Phys. Rev. Lett.* **90**, 031301 (2003) [arXiv:astro-ph/0207517].
- [46] Y. Wang and M. Tegmark, *Phys. Rev. Lett.* **92**, 241302 (2004) [arXiv:astro-ph/0403292].
- [47] U. Alam, V. Sahni and A. A. Starobinsky, *JCAP* **0406**, 008 (2004) [arXiv:astro-ph/0403687].
- [48] Y. Wang and P. Mukherjee, *Astrophys. J.* **606**, 654 (2004) [arXiv:astro-ph/0312192].

- [49] U. Alam, V. Sahni, T. D. Saini and A. A. Starobinsky, *Mon. Not. Roy. Astron. Soc.* **354**, 275 (2004) [arXiv:astro-ph/0311364].
- [50] T. Padmanabhan and T. R. Choudhury, *Mon. Not. Roy. Astron. Soc.* **344**, 823 (2003) [arXiv:astro-ph/0212573].
- [51] Z. H. Zhu, M. K. Fujimoto and X. T. He, *Astron. Astrophys.* **417**, 833 (2004) [arXiv:astro-ph/0401095].
- [52] M. Chevallier and D. Polarski, *Int. J. Mod. Phys. D* **10**, 213 (2001)
- [53] E. V. Linder, *Phys. Rev. Lett.* **90**, 091301 (2003)
- [54] B. Feng, X. L. Wang and X. M. Zhang, *Phys. Lett. B* **607**, 35 (2005) [arXiv:astro-ph/0404224].
- [55] S. Hannestad and E. Mortsell, *JCAP* **0409**, 001 (2004) [arXiv:astro-ph/0407259].
- [56] J. Q. Xia, B. Feng and X. M. Zhang, *Mod. Phys. Lett. A* **20**, 2409 (2005) [arXiv:astro-ph/0411501].
- [57] J. Q. Xia, G. B. Zhao, B. Feng, H. Li and X. Zhang, *Phys. Rev. D* **73**, 063521 (2006) [arXiv:astro-ph/0511625].
- [58] J. Q. Xia, G. B. Zhao, B. Feng and X. Zhang, *JCAP* **0609**, 015 (2006) [arXiv:astro-ph/0603393].
- [59] G. B. Zhao, J. Q. Xia, B. Feng and X. Zhang, *Int. J. Mod. Phys. D* **16**, 1229 (2007) [arXiv:astro-ph/0603621].
- [60] J. Q. Xia, G. B. Zhao, H. Li, B. Feng and X. Zhang, *Phys. Rev. D* **74**, 083521 (2006) [arXiv:astro-ph/0605366].
- [61] J. Q. Xia, G. B. Zhao and X. Zhang, *Phys. Rev. D* **75**, 103505 (2007) [arXiv:astro-ph/0609463].
- [62] G. B. Zhao, J. Q. Xia, H. Li, C. Tao, J. M. Virey, Z. H. Zhu and X. Zhang, *Phys. Lett. B* **648**, 8 (2007) [arXiv:astro-ph/0612728].
- [63] Y. Wang and P. Mukherjee, *Phys. Rev. D* **76**, 103533 (2007) [arXiv:astro-ph/0703780].
- [64] E. L. Wright, *Astrophys. J.* **664**, 633 (2007) [arXiv:astro-ph/0701584].
- [65] H. Li, J. Q. Xia, G. B. Zhao, Z. H. Fan and X. Zhang, *Astrophys. J.* **683**, L1 (2008) [arXiv:0805.1118 [astro-ph]].
- [66] J. Q. Xia, H. Li, G. B. Zhao and X. Zhang, *Phys. Rev. D* **78**, 083524 (2008) [arXiv:0807.3878 [astro-ph]].
- [67] H. Li *et al.*, arXiv:0812.1672 [astro-ph].

- [68] E. Komatsu *et al.* [WMAP Collaboration], *Astrophys. J. Suppl.* **180**, 330 (2009) [arXiv:0803.0547 [astro-ph]].
- [69] Y. F. Cai, E. N. Saridakis, M. R. Setare and J. Q. Xia, arXiv:0909.2776 [hep-th].
- [70] G. B. Zhao, J. Q. Xia, M. Li, B. Feng and X. Zhang, *Phys. Rev. D* **72**, 123515 (2005) [arXiv:astro-ph/0507482].
- [71] C. P. Ma and E. Bertschinger, *Astrophys. J.* **455**, 7 (1995) [arXiv:astro-ph/9506072].
- [72] D. Wands, K. A. Malik, D. H. Lyth and A. R. Liddle, *Phys. Rev. D* **62**, 043527 (2000) [arXiv:astro-ph/0003278].
- [73] M. Kawasaki, T. Moroi and T. Takahashi, *Phys. Rev. D* **64**, 083009 (2001) [arXiv:astro-ph/0105161].
- [74] T. Moroi and T. Takahashi, *Phys. Rev. Lett.* **92**, 091301 (2004) [arXiv:astro-ph/0308208].
- [75] C. Gordon and D. Wands, *Phys. Rev. D* **71**, 123505 (2005) [arXiv:astro-ph/0504132].
- [76] A. Lewis, A. Challinor and A. Lasenby, *Astrophys. J.* **538**, 473 (2000) [arXiv:astro-ph/9911177].
- [77] J. Weller and A. M. Lewis, *Mon. Not. Roy. Astron. Soc.* **346**, 987 (2003) [arXiv:astro-ph/0307104].
- [78] R. R. Caldwell, R. Dave and P. J. Steinhardt, *Phys. Rev. Lett.* **80**, 1582 (1998) [arXiv:astro-ph/9708069].
- [79] A. G. Riess *et al.* [Supernova Search Team Collaboration], *Astrophys. J.* **607**, 665 (2004) [arXiv:astro-ph/0402512].
- [80] C. R. Contaldi, M. Peloso, L. Kofman and A. Linde, *JCAP* **0307**, 002 (2003) [arXiv:astro-ph/0303636].
- [81] B. Feng and X. Zhang, *Phys. Lett. B* **570**, 145 (2003) [arXiv:astro-ph/0305020].
- [82] A. Kogut *et al.* [WMAP Collaboration], *Astrophys. J. Suppl.* **148**, 161 (2003) [arXiv:astro-ph/0302213].
- [83] G. Hinshaw *et al.* [WMAP Collaboration], *Astrophys. J. Suppl.* **148**, 135 (2003) [arXiv:astro-ph/0302217].
- [84] S. Dodelson, *Amsterdam, Netherlands: Academic Pr. (2003) 440 p.*
- [85] B. Jain and A. Taylor, *Phys. Rev. Lett.* **91**, 141302 (2003) [arXiv:astro-ph/0306046].

- [86] P. Zhang and U. L. Pen, *Mon. Not. Roy. Astron. Soc.* **367**, 169 (2006) [arXiv:astro-ph/0504551].
- [87] P. Zhang and U. L. Pen, *Phys. Rev. Lett.* **95**, 241302 (2005) [arXiv:astro-ph/0506740].
- [88] Coley A. A., “Dynamical systems and cosmology,” *Kuwer Academic Publishers, (2003)*.
- [89] R. J. van den Hoogen and L. Filion, “Stability analysis of multiple scalar field cosmologies with matter,” *Class. Quant. Grav.* **17**, 1815 (2000).
- [90] A. A. Coley and R. J. van den Hoogen, “The dynamics of multi-scalar field cosmological models and assisted inflation,” *Phys. Rev. D* **62**, 023517 (2000) [arXiv:gr-qc/9911075].
- [91] R. Tavakol, “Introduction to dynamical systems,” *ch. 4, Part one, pp. 84–98, Cambridge University Press, Cambridge, England, 1997*.
- [92] Y. Leyva Nodal, V. F. Cardone, and R. P. Cardenas, *AIP Conf. Proc.* **1083** (2008) 128–135.
- [93] M. Fukugita and P.J.E Peebles, *ApJ*, 616, 643, 2004.
- [94] D. Eisenstein et al., *ApJ*, 633, 560, 2005.
- [95] M.A. Strauss et al., *AJ*, 124, 1810, 2002.
- [96] J.R. Bond, G. Efstathiou, M. Tegmark, *MNRAS*, 291, L33, 1997.
- [97] Y. Leyva, R. Cardenas, and V. Cardone, *Astrophys. Space Sci.* **323** (2009) 107.